Fall 2014

# Spatial relationship between GPS slip and seismic tremor during Cascadia slow slip events

Hillary Lynn Goodner
*Central Washington University*

# SPATIAL RELATIONSHIP BETWEEN GPS SLIP AND SEISMIC TREMOR DURING CASCADIA SLOW SLIP EVENTS

---

A Thesis

Presented to

The Graduate Faculty

Central Washington University

---

In Partial Fulfillment

of the Requirements for the Degree

Master of Science

Geology

---

by

Hillary Lynn Goodner

December 2014

CENTRAL WASHINGTON UNIVERSITY

Graduate Studies

We hereby approve the thesis of

Hillary Lynn Goodner

Candidate for the degree of Master of Science

APPROVED FOR THE GRADUATE FACULTY

_____ _____
Dr. Walter M. Szeliga, Committee Chair

_____ _____
Dr. Timothy I. Melbourne

_____ _____
Dr. Anne E. Egger

_____ _____
Dean of Graduate Studies

ABSTRACT

SPATIAL RELATIONSHIP BETWEEN GPS SLIP AND SEISMIC TREMOR DURING CASCADIA SLOW SLIP EVENTS

by

Hillary Lynn Goodner

December 2014

We model GPS deformation and timing of seismic tremor associated with transient deformation in Cascadia to test the hypothesis that tremor and slip occur synchronously but are spatially offset. For the period 2010–2013, we use seismic tremor data with a duration-moment relationship to predict GPS time series and compare them to observations. We find that observed GPS displacements are best predicted when tremor locations on the plate interface are shifted 15 km up-dip of their published epicenter. To test whether the spatial offset of tremor and slip is due to systematic mislocation of published epicenters, we attempt to identify individual sources of tremor using Independent Component Analysis. However, our results are inconclusive. Additionally, our results suggest a moment rate lower than previous studies. We propose that increases in instrumentation have resulted in an increase in recorded tremor giving the appearance of a decrease in moment rate.

ACKNOWLEDGMENTS

I would like to thank the NASA ROSES-NNX10AD15G grant for supporting this research. I acknowledge PANGA and MEASURES processing centers as my source for GPS data used in my study. I acknowledge the PNSN as my source for seismic tremor data. I would like to thank the Geological Sciences Department at CWU for the opportunity to pursue a Masters degree, especially my advisor, Dr. Walter Szeliga, for his patience, encouragement, and support throughout the process. I would also like to thank my family and friends for their continued support and encouragement, especially my husband, Chris.

TABLE OF CONTENTS

LIST OF FIGURES

LIST OF FIGURES CONTINUED

# CHAPTER I

## INTRODUCTION

The Pacific Northwest is home to the Cascadia Subduction Zone (CSZ), a 1,100-km long fault zone that runs from central Vancouver Island, BC, Canada to northern California, USA [*Miller et al.*, 2002] (Figure 1). This zone marks the convergent boundary between the oceanic Juan de Fuca plate and the North American continental plate resulting in the volcanic arc of the Cascades and the subduction trench. A less apparent effect of the subduction zone is strain accumulation. The net northeast motion of the Juan de Fuca plate relative to the North America plate is 3.5-4.5 cm per year at the Pacific coast [*Heaton and Hartzell*, 1987]. The resulting strain accumulated on the subduction zone has been released in great earthquakes in the past, such as an event in 1700, which could happen again.

Subduction zones, in general, release significant amounts of energy during megathrust earthquakes (earthquakes with $M_W > 8$). In fact, about 85% of all energy released by earthquakes globally between 1906 and 1986 occurred in subduction zones [*Scholz*, 1990]. Large megathrust earthquakes have occurred numerous times in the instrumental period, for example, the $M_w$ 9.5 Chile earthquake in 1960, $M_w$ 9.2 Alaska earthquake in 1964, $M_w$ 9.1 Sumatra earthquake in 2004, and the $M_w$ 9.0 Japan earthquake in 2011. It is no longer seen as rare for subduction zones to rupture great lengths and produce earthquakes larger than magnitude 9. Recognizing that the CSZ is also capable of producing a magnitude 9 earthquake has led to a new focus on hazards monitoring and risk mitigation in the Pacific Northwest. However, megathrust

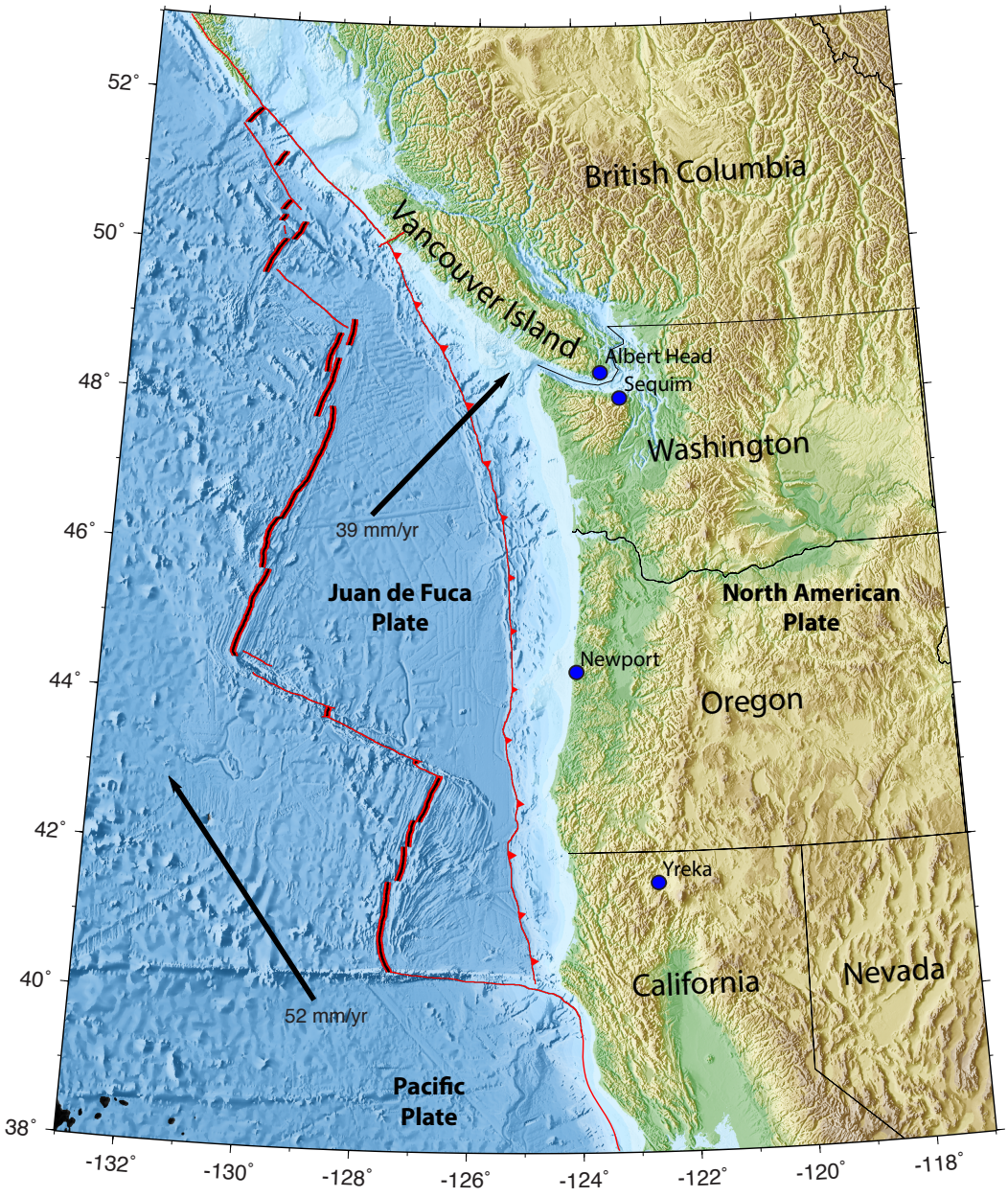


Figure 1: The 1,100 km long Cascadia Subduction zone (line with teeth) is located in the Pacific Northwest region of the United States. It is comprised of the oceanic Juan de Fuca plate subducting beneath the North America plate at a rate of 3-4 cm/yr. The northern portion of the subduction zone extends from the Oregon-Washington border northward to Vancouver Island. Locations mentioned in the text are indicated by blue dots. Red and black striped lines represent spreading centers and thin red lines represent transforms faults. Plate motion vectors are relative to stable North America.

earthquakes are not the only ways in which stored strain may be released in a subduction zone.

Other processes have been recorded in the past 20 years by seismic and geodetic instruments, including tremor, aseismic slip, and seismic slip. Some events, such as Episodic Tremor and Slip (ETS), occur imperceptibly. These events, also known as slow earthquakes or silent earthquakes, occur on a different time scale than typical earthquakes. While typical earthquakes rupture within seconds to, at most, minutes, the rupture time for ETS events is several weeks. Since ETS events occur over a long time period, no shaking is felt at the surface even though they release the energy equivalent to a ~$M_W$ 6.6 or larger. However, no perceptible shaking does not imply no motion on the surface. GPS stations record their locations in space and time very accurately, which provides a useful tool to measure this motion on the surface. This motion is referred to as surface deformation. It is projected onto the fault interface in order to estimate the amount of fault slip occurring during each event. While surface deformation is typically less than 0.5 cm over seven days, this surface deformation, projected onto the CSZ fault interface, translates to approximately 5 cm of fault slip.

Seismic data also provide insight into ETS events. The very high resolution, short time scale measurements recorded by seismometers can also be used to study different aspects of ETS events. Non-volcanic tremor is a seismic phenomenon that lacks impulsive P- and S-wave arrivals. Processing seismic data by filtering allows the location and duration to be determined. While it is believed that these tremors originate near the plate interface, this has yet to be conclusively demonstrated. What is known,

however, is that non-volcanic tremor and surface deformation occur contemporaneously. This coincidence defines ETS.

How strain accumulates in a subduction zone depends primarily on temperature and rock strength [*Pacheco et al.*, 1993; *Hyndman and Wang*, 1993]. By temperature and pressure increasing down-dip along the subduction interface, we may partition the behavior of the plate interface into a series of zones (Figure 2). The uppermost and coldest zone is referred to as the seismogenic, or locked, zone, and extends from near the surface to roughly 30 km depth [*Hyndman and Wang*, 1993; *Nedimović et al.*, 2003]. Most earthquakes, including megathrust events, are known to occur in this shallow zone. At much greater depths, the increase in temperature prevents strain accumulation and therefore seismic rupture; a zone known as the aseismically slipping region [*Hyndman and Wang*, 1993; *Nedimović et al.*, 2003]. This region is where the subducting plate rides smoothly and freely past the overriding plate. The transition between these two zones must be gradual; otherwise a large strain gradient between the seismogenic and aseismically slipping regions of the subduction zone would exist. This region is known as the transition zone, and is located below the seismogenic zone, and extends to approximately 45 km depth [*Hyndman and Wang*, 1993; *Nedimović et al.*, 2003]. Research thus far suggests that ETS events occur in this zone. The occurrence of ETS events in the transition zone suggests that they transfer stress from the aseismic to the seismogenic zone; bringing the fault closer to failure, resulting in the next earthquake possibly similar to the 1700 event [*Rogers and Dragert*, 2003].

The uncertainty in the precise timing and location of both slip and tremor phenomena may provide clues to the underlying behavior of the transition zone. The motivation for my research is the current lack of tremor depth resolution. Further constraining this measurement would greatly impact the knowledge of how tremor and slip are spatially related and whether they are two separate phenomena produced during ETS events. I will examine the spatial relationship between tremor and slip during ETS events occurring in 2010, 2011, 2012, and 2013 in the northern portion of the CSZ to resolve these fundamental questions pertaining to ETS.

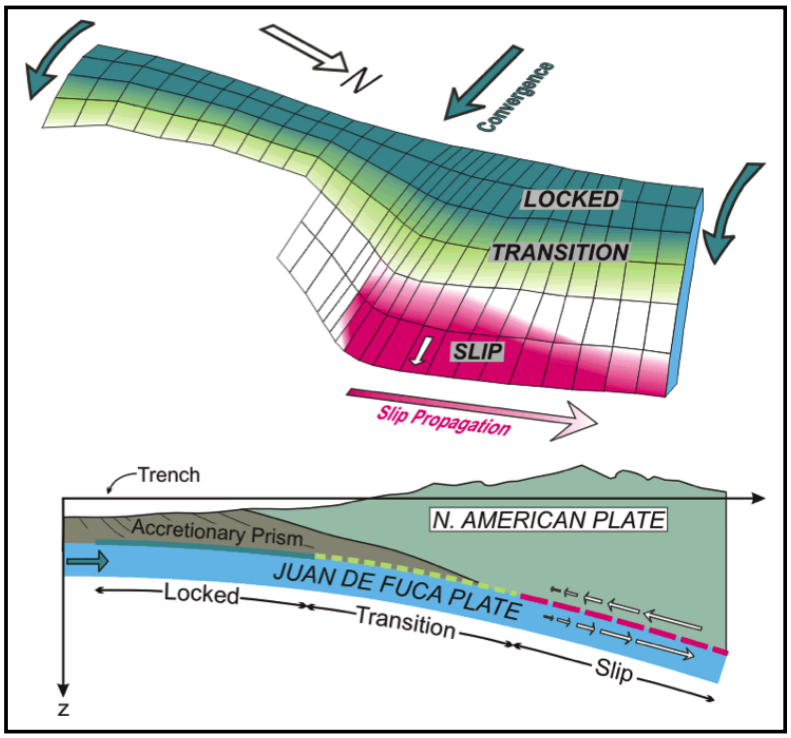


Figure 2: Three-dimensional view of the subducting Juan de Fuca plate interface. Temperature and pressure increase with depths, which has a direct effect on rock strength. Three zones of fault behavior may be defined: The locked, or seismogenic, zone is located near the surface and extends approximately 30 km down-dip. This zone is where the majority of earthquakes rupture. The freely slipping, or aseismic, zone is the deepest zone where the plates slide past each other with little resistance. In between these two zones lies the transition zone. Here, the conditions are such that the fault is not fully locked and may allow rupture to occur, particularly during ETS events. Image courtesy of S. Beck, unpublished.

# CHAPTER II

# BACKGROUND

Prior to modern instrumentation, and for most of the twentieth century, the CSZ was not thought to produce large earthquakes, especially nothing as large as recent earthquakes in Japan and Sumatra. Up through the 1980's the CSZ was believed to slip aseismically primarily due to the lack of recorded earthquakes along the boundary [*Heaton and Kanamori*, 1984]. Although the region is home to many native tribes, written records were not kept. Some of their oral histories refer to events that could be interpreted as tsunamis, suggesting that this region has been seismically active [*Heaton and Snavely*, 1985]. Evidence for large megathrust earthquakes in the Pacific Northwest in the form of ghost forests, tsunami deposits, and other coastal subsidence features was eventually uncovered in the late 1980's [*Atwater*, 1987].

Further research in the 1990's also uncovered reports of a tsunami in Japan with no known parent earthquake, an event termed an orphan tsunami, during the year 1700 [*Atwater et al.*, 2005]. Correlations between radiocarbon dating, tree ring analysis, and dating of tsunami deposits, along with written records from Japan, led to the conclusion that the orphan tsunami was the result of a megathrust earthquake on the CSZ [*Atwater et al.*, 2005]. These observations of coastal subsidence, in particular, demonstrated that the subduction zone had been active during the Holocene, a finding that led Atwater [1987] to warn others that seismic hazard in the CSZ should not be ignored. Further refinement of coastal subsidence and tsunami deposit mapping has suggested that large earthquakes are, in fact, common, with a recurrence interval of approximately 530 years [*Adams*,

1990; *Flück et al.*, 1997; *Atwater and Hemphill-Haley*, 1997; *Witter et al.*, 2003; *Goldfinger et al.*, 2003; *Nelson et al.*, 2006].

By the early 1990's, a new geodetic network, PANGA, was being installed to measure surface deformation (and thus strain accumulation) in the Pacific Northwest as a result of subduction. This geodetic network was originally established in order to estimate strain accumulation in the CSZ, however, the network also recorded many other processes, including small, short duration reversals of motion that had not been previously observed. The data recorded by the PANGA network led to the discovery of regularly repeating, small amplitude surface displacements roughly a decade after the network was installed [*Dragert et al.*, 2001; *Miller et al.*, 2002; *Rogers and Dragert*, 2003].

While geodesists were beginning to recognize periodic surface displacements from slow earthquakes, seismologists were studying a different phenomena. Seismic measurements can range over a wide span of frequencies, causing interesting signals can often be hidden. Some signals that are recorded, such as wind and ocean microseisms, can mask other interesting signals. An example of an interesting signal that can be masked by other noise sources is volcanic tremor which is the low frequency (1-9 Hz) vibration produced by activity within a magma chamber [*Beroza and Ide*, 2011]. Although the CSZ region contains active volcanoes that produce volcanic tremor, seismometers also record tremor not related to volcanic systems, referred to as non-volcanic tremor. In contrast to volcanic tremor, non-volcanic tremor often consists of high frequency (1-5 Hz) elastic waves. Similar to volcanic tremor, however, non-

volcanic tremor is easily hidden among typical background noise and can be revealed by filtering the data. In southeastern Japan, Obara [2002] observed these high frequency tremor signals occurring in a region where no volcanoes were present; coining the term non-volcanic tremor to describe this phenomena. While non-volcanic tremor resembles seismic noise and does not appear to contain body wave phases (P- and S-wave arrivals), the source is nonetheless believed to be tectonic [*Obara*, 2002; *Aguiar et al.*, 2009]. Rogers and Dragert [2003] identified similar signals in northern Cascadia to those found in Japan. Their analysis indicated that non-volcanic tremor appeared contemporaneous with geodetically measured slow earthquakes, and thus they coined the phrase episodic tremor and slip, or ETS.

ETS events have since been found to occur at other subduction zones [*Gomberg et al.*, 2010]. The significance of ETS events in the seismogenic cycle of a subduction zone is still unclear. However, due to the location of the GPS stations recording the surface deformation, approximately 100 km from the trench, we understood that these events occur down-dip of the seismogenic, or locked, zone along the fault interface, potentially applying additional stress to the locked zone. This stress loading could bring the fault closer to failing resulting in a megathrust earthquake [*Rogers and Dragert*, 2003].

Further examination of geodetic and seismic data along the length of the CSZ demonstrated that ETS events not only occur in the northern portion of the CSZ but also in the southern portion (refer to Figure 1), but with varying recurrence intervals of between 10 and 14 months [*Szeliga et al.*, 2004]. During the 18-23 days, dependent upon

each event, when surface deformation was observed, seismic stations also recorded a spike in the number of hours of tremor per week, providing a strong temporal correlation between tremor and slip phenomena (Figure 3). By studying a total of 23 slow slip events with corresponding tremor data, Aguiar et al. [2009] identified a linear correlation between GPS-inferred moment and the number of hours of tremor observed (Figure 4).

My research refines the spatial and temporal correlation between surface deformation and non-volcanic tremor. I began by determining the location on the fault interface that slip occurred during each of the four ETS events that I studied. I further the understanding of the spatial relationship between tremor and slip during ETS events by employing a moment-rate function to predict actual GPS measurements from non-volcanic tremor data. If tremor and slip are truly co-located, I should have been able to reproduce the observed GPS surface deformation. I also attempted to determine P- and S- wave arrivals on individual tremor signals by using independent component analysis (ICA). To date, the ICA algorithm has not been applied to seismic data. Below is a description of the methods I used to achieve this goal.

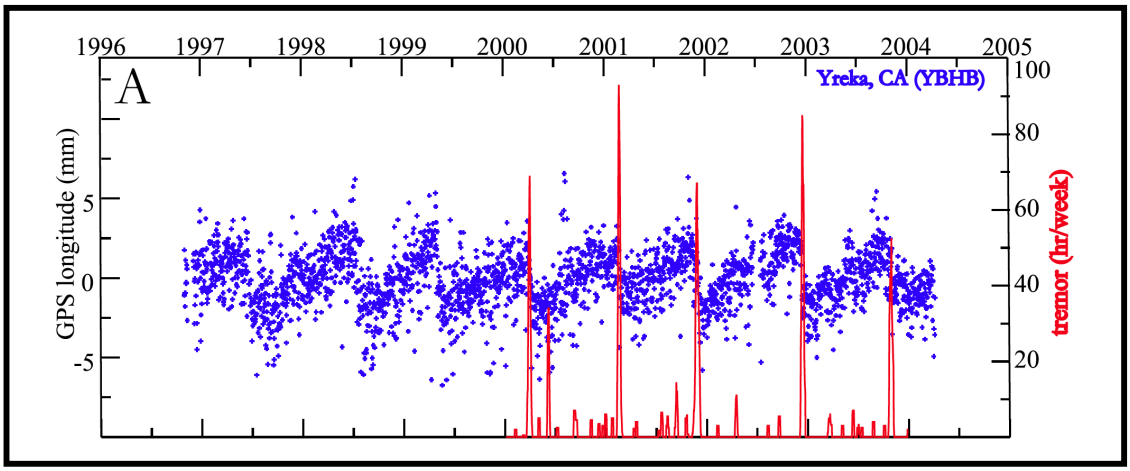


Figure 3: Hours of tremor per week plotted as a function of time along with eastward GPS displacement at Yreka, California. Spikes in tremor coincide with surface displacement, a behavior characteristic of ETS. Figure modified from Szeliga et al., 2004. See Figure 1 for lcoations.

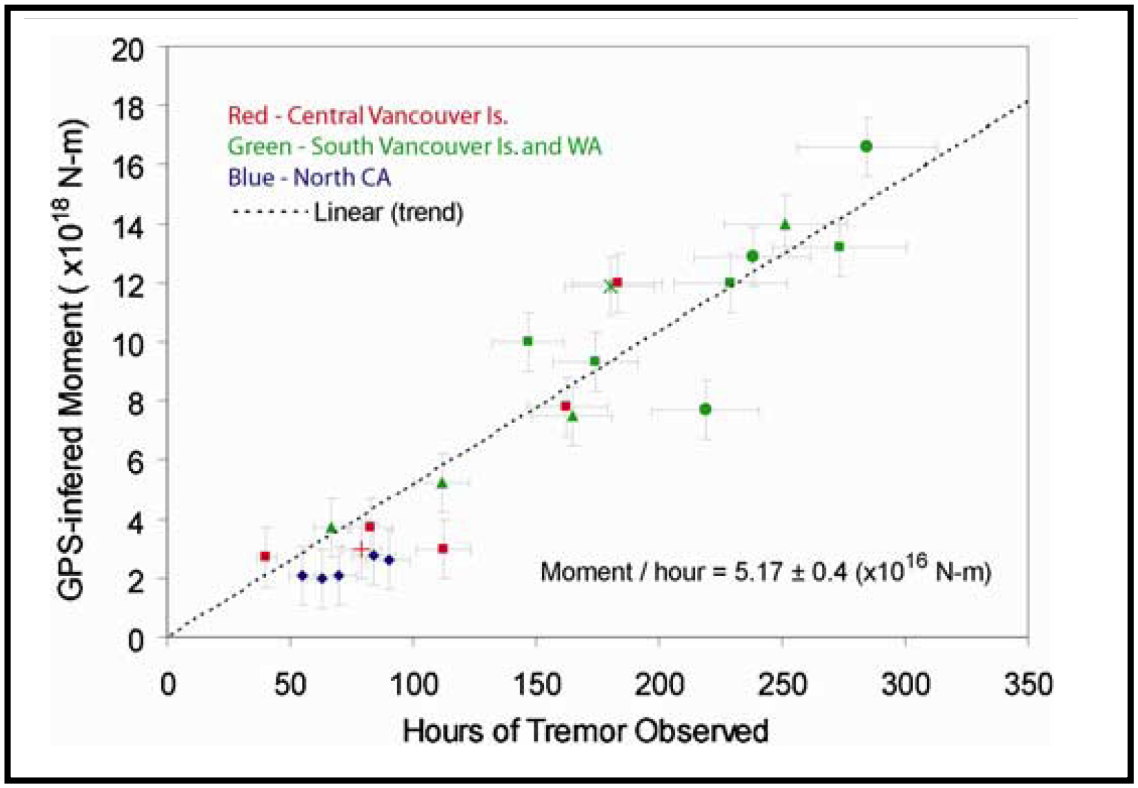


Figure 4: GPS-inferred moment plotted against hours of observed tremor for different portions of the Cascadia subduction zone. A moment-rate of 5.17 x $10^{16}$ N-m per hour provides a reasonable fit to the data and is used in this paper. The linear trend observed allows one to estimate moment for short durations of tremor. Figure modified from Aguiar et al., 2009.

## Methods

I retrieved surface displacement data from 33-55 GPS stations located in northern Cascadia, between central Vancouver Island, BC, to southern Washington, all west of the Cascade Mountain range (see data tables in Appendix). The timeframe of the data was August 15–December 15, 2010, August 15–December 15, 2011, June 10–October 11, 2012, and July 15–November 15, 2013 in order to analyze the 2010, 2011, 2012, and 2013 events, respectively. Data from GPS provides a record of transient surface deformation caused by slip along the megathrust at depth, and inversion of these measurements yields information about the moment (energy released) and amount of slip that occurred for each event. Prior to inverting the data for slip, a model of the fault interface is divided into equal sized sections to simplify computation [Szeliga et al., 2008; Chapman and Melbourne, 2009; Aguiar et al., 2009]. In this inversion, elastic Greens functions are used to approximate the behavior of the lithosphere between the instrument and the fault interface. The elastic Greens functions provide a set of solutions that represent the relationship between sections of the fault interface and motion of each GPS station in both the north and east components. A Laplacian smoothing operator was also utilized to reduce any large, non-physical strain gradients that result from inversion of sparse surface displacement data [Melbourne et al., 2003]. These assumptions allowed me to not only calculate the moment of each ETS event, but also determine the location of slip on the fault interface during each event. From my inversions, I created two visualizations for each event; the first is a map of displacement vectors for each GPS station. The second is a slip distribution diagram showing slip on the plate interface.

I then analyzed seismic data recorded on approximately 200 seismometers by the PNSN located between central Vancouver Island, BC and southern Washington. During my analysis, I employed two methods: by firstly calculating synthetic GPS measurements derived from tremor data and comparing it to actual GPS measurements. Secondly, by decomposing tremor signals to determine whether simpler waveforms can be extracted. I used tremor locations and durations as a proxy for slip location and amount, and modeled the resulting surface deformation as a function of time.

The final analysis for my research used seismic data recorded by eight broadband seismometers that were installed prior to the 2010 ETS event. The campaign network was a small aperture array in the northeastern region of the Olympic Peninsula near Sequim, WA (Figure 5). I used independent component analysis (ICA) on the tremor data in an attempt to identify individual body-wave phase signals from tremor. ICA is a signal processing strategy used to separate statistically independent signals in a data set [Comon, 1994; Hyvarinen, 1999; Hyvarinen and Oja, 2000].

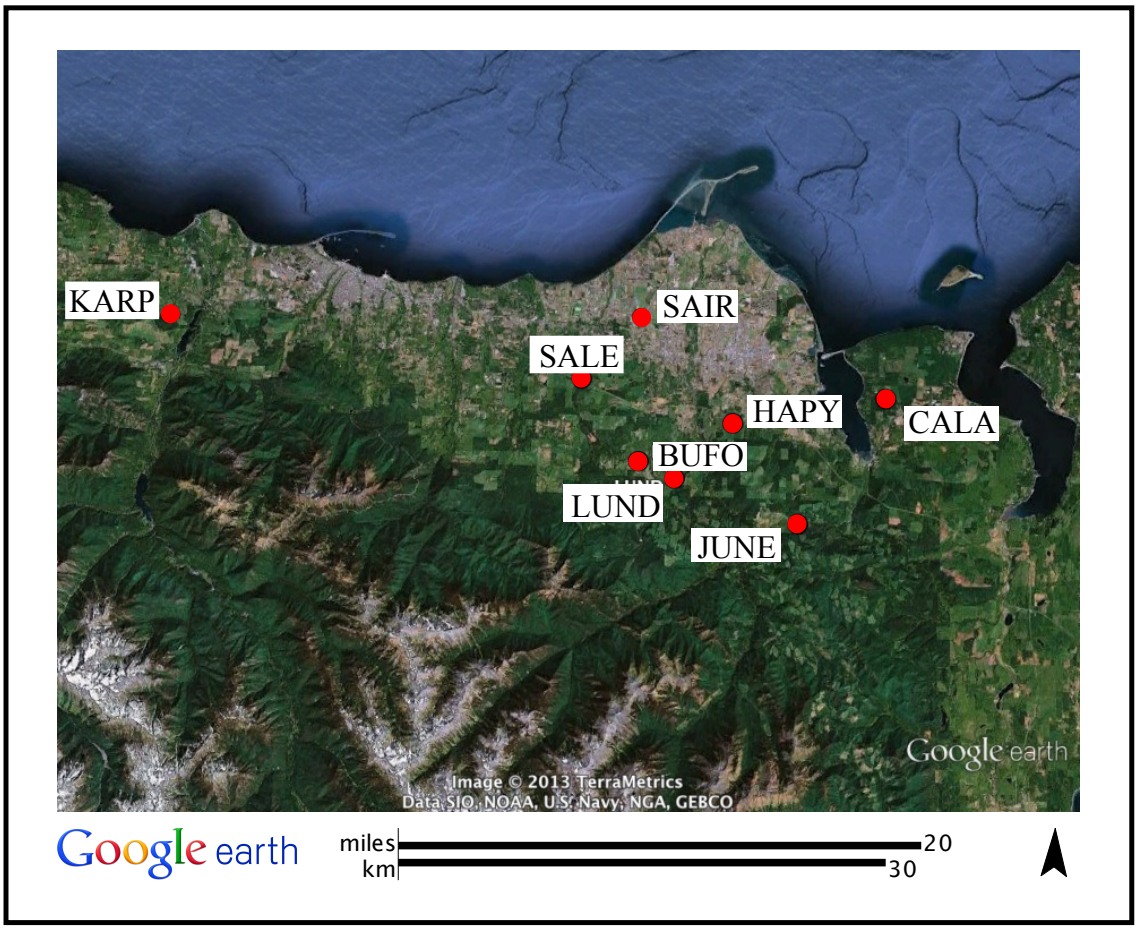


Figure 5: The campaign network of eight broadband seismic stations centered about Sequim, WA. These seismic stations were deployed for two months in late summer 2010 and recorded tremor data during the 2010 ETS event. Refer to Figure 1 for the location of Sequim, WA.

# CHAPTER III

# JOURNAL ARTICLE

## 1. Introduction

The principal source of moment release in a subduction zone comes from large (exceeding magnitude 9.0), infrequent (recurrence intervals of hundreds of years) megathrust earthquakes. In Cascadia (Figure 1), these earthquakes recur approximately every 530 years with the most recent earthquake occurring on 26 January 1700 estimated at $M_w$ 9.0 [*Adams*, 1990; *Atwater*, 1992; *Flück et al.*, 1997; *Atwater and Hemphill-Haley*, 1997; *Satake et al.*, 2003; *Witter et al.*, 2003; *Goldfinger et al.*, 2003]. Since the installation of continuous geodetic monitoring in Cascadia in the late 1990's, other sources of moment release have been observed. One of these sources is referred to as Episodic Tremor and Slip (ETS) events and consists of slow (two-week duration) slip on the plate interface accompanied by increased high frequency seismic noise, a signal termed non-volcanic tremor [*Rogers and Dragert*, 2003].

While the temporal correlation between tremor and slip is strong [*Rogers and Dragert,* 2003; *Kao et al.*, 2009; *Beroza and Ide*, 2011], the physical relationship between these processes is still poorly understood [*Segall et al.*, 2010]. One assumption about the relationship between slip and tremor is that they are two aspects of the same process and occur in a truly simultaneous manner, on or near the plate interface. To test this assumption, we will use tremor locations and durations as a proxy for slip, and model the resulting surface deformation as a function of time. If our assumption of true

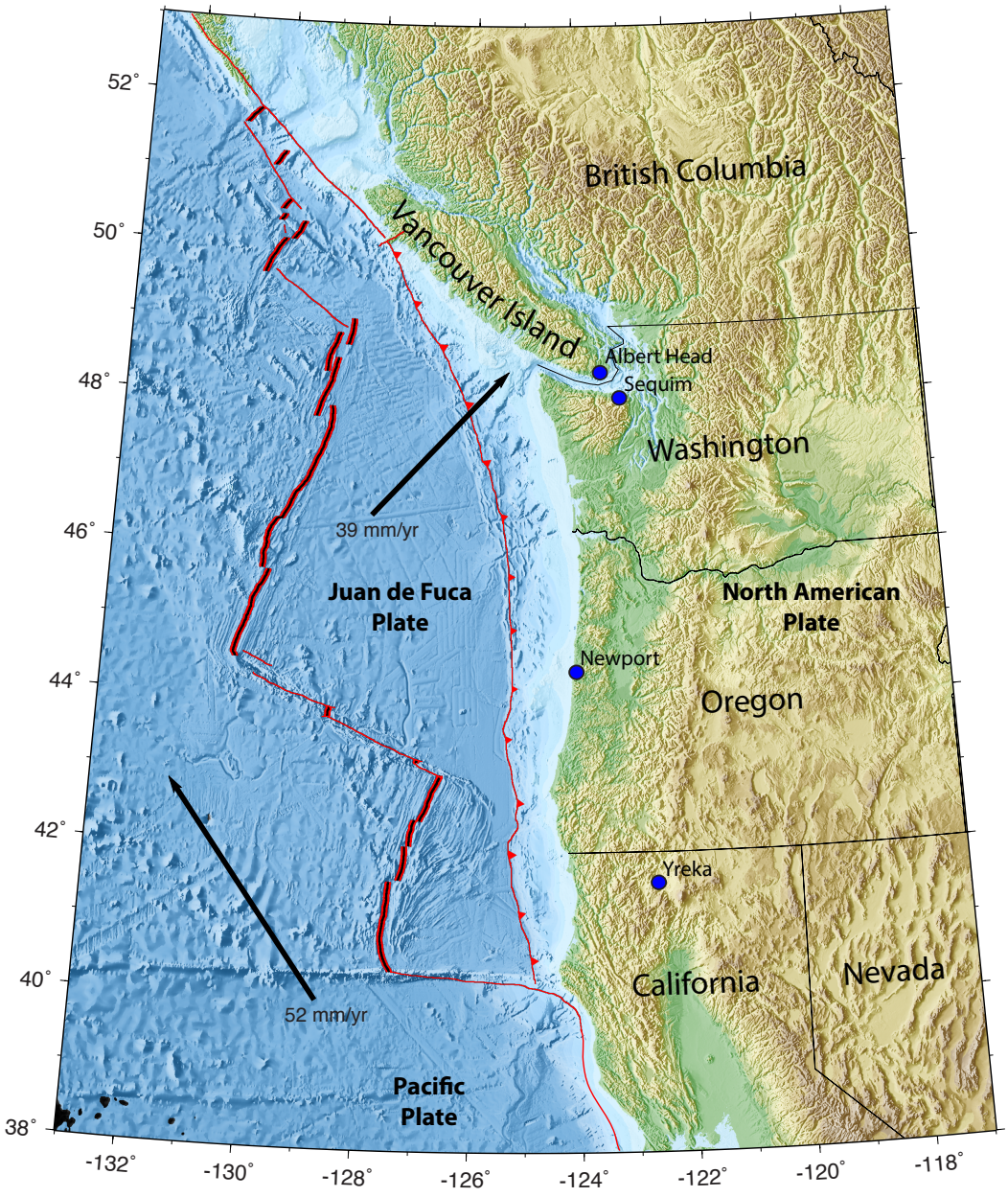


Figure 1: The 1,100 km long Cascadia Subduction zone (line with teeth) is located in the Pacific Northwest region of the United States. It is comprised of the oceanic Juan de Fuca plate subducting beneath the North America plate at a rate of 3-4 cm/yr. The northern portion of the subduction zone extends from the Oregon-Washington border northward to Vancouver Island. Locations mentioned in the text are indicated by blue dots. Red and black striped lines represent spreading centers and thin red lines represent transforms faults. Plate motion vectors are relative to stable North America.

simultaneity and co-location are correct, we should be able to reproduce all, or nearly all, of the observed surface deformation observed in the GPS signal. We will focus on four ETS events occurring between 2010 and 2013 in northern Cascadia to address the relationship between tremor and slip.

To begin, we use tremor epicenters and durations from approximately 200 stations in the Pacific Northwest Seismic Network (PNSN) [*Wech and Creager*, 2008] to calculate the depth to the plate interface using a model for the Juan de Fuca plate interface from McCrory et al. [2012]. Assuming each burst of tremor may be approximated as a point source and located on the plate interface, we use a linear moment-versus-duration model [*Aguiar et al.*, 2009] to forward model the surface deformation as a function of time, generating synthetic time series. We then compare these synthetic time series to geodetic observations from the Plate Boundary Observatory (PBO) and Pacific Northwest Geodetic Array (PANGA).

In order to compare possible differences in the location of tremor and slip for the events under study, we also calculate slip locations from GPS offsets using the methods outlined in Szeliga et al. [2008]. In addition, we attempt to separate individual sources of tremor using independent component analysis (ICA) with data recorded during 2010 from a dense seismic array on the Olympic Peninsula to constrain the location of tremor. The result of this work can be applied to subduction zones around the world in order to determine P- and S- wave arrivals to better locate seismic tremor during future events.

## 1.1 ETS in northern Cascadia

The occurrence of transient deformation events in Cascadia was first recognized in 1999, when seven GPS stations located in northwestern Washington captured a short duration (two-week) reversal of secular motion [*Dragert et al.*, 2001; *Miller et al.*, 2002]. The secular motion for the region is approximately 3-4 cm/yr to the northeast, however, during this short duration reversal, the motion was to the southwest with a magnitude of about 0.3-0.4 cm. The relatively sparse network of GPS stations during this time period made identification of the source of the transient deformation difficult. During the early 2000's, prior to the installation of the Plate Boundary Observatory, the spatial density of GPS stations improved and by 2003 the density of surface observations had improved enough to provide confidence that the observed transient deformation had an origin at or near the plate interface [*Melbourne et al.,* 2005].

During this time period, high-frequency (1–5 Hz) seismic noise that resembled tremor associated with magma movement in volcanic settings was observed but did not appear to be closely associated with volcanism, the phenomenon was termed non-volcanic tremor [*Obara*, 2002]. Rogers and Dragert [2003] analyzed these tremor-like signals and deemed them uncorrelated to local earthquakes and demonstrated that, in an aggregate sense, they occur contemporaneously with geodetic slow slip in Cascadia. This contemporaneous occurrence of non-volcanic tremor and geodetic slip was termed Episodic Tremor and Slip (ETS) [*Rogers and Dragert*, 2003]. While continuous, high-precision geodetic measurements were not available prior to 1997 in the Pacific Northwest, evidence for recurrence of non-volcanic tremor approximately every 14-

months has been found in seismic paper records, and suggests their regular occurrence back to at least 1987 [*Rogers*, 2007].

In northern Cascadia, ETS events are observed approximately every 14 months as brief (4- to 6-week) reversals in secular motion recorded by GPS [*Miller et al.*, 2002; *Szeliga et al.*, 2004; *Melbourne et al.,* 2005; *Creager and Melbourne*, 2007; and others]. During the four to six week duration of each event, rupture appears to propagate along strike of the subducting Juan de Fuca plate [*Dragert et al.*, 2001; *Miller et al.*, 2002] and results in an equivalent moment release of approximately $M_W$ 6.7 [*Dragert et al.*, 2001; *Miller et al.*, 2002; *Melbourne et al.*, 2005; *Szeliga et al.*, 2008]. During these events, a temporal relationship between the duration of non-volcanic tremor and the resultant geodetic moment exists. Aguiar et al. [2009] investigated the correlation and found a linear relationship exists; $5.17 \times 10^{16}$ N-m of energy is released during each hour of tremor. This contemporaneous occurrence of tremor and slip suggest that they are manifestations of the same process but, until now, no direct connection between the two phenomena has been shown [*Wech and Creager*, 2007]. In this study, we are interested in constraining the spatial relationship of these two manifestations.

Because they are so common, ETS events are key to understanding the processes of subduction zones, such as the segmentation of the seismogenic zone in Cascadia [*Szeliga et al.*, 2004] and stress loading of the locked seismogenic zone [*Dragert et al.*, 2001; *Rogers and Dragert*, 2003; *Melbourne and Webb*, 2003; *Ito et al.*, 2012]. An understanding of stress loading is particularly important, since it is still unknown whether

it is possible for an ETS event to trigger a great earthquake in the locked portion of a subduction zone [*Dragert et al.*, 2001; *Rubinstein et al.*, 2009].

## 2. Spatial relationship of tremor and slip

On a gross scale, tremor and slip occur contemporaneously during ETS events in Cascadia [*Rogers and Dragert*, 2003; *Melbourne and Webb*, 2003; *Szeliga et al.*, 2004; *Aguiar*, 2007 and others]. We are interested in refining this temporal correlation and further constraining how these two processes are spatially related. To do this, we modeled ETS events during 2010–2013 using PANGA and MEASURES processed GPS data along with tremor data from the PNSN [*Wech,* 2010].

Aguiar et al. [2009] examined 11 years (1997–2008) of ETS events that occurred margin-wide to compare the moment release to the duration of non-volcanic tremor during ETS events. Aguiar et al. [2009] determined that a linear relationship exists between the duration of non-volcanic tremor (hours of continuous tremor) and the moment released by the slip. This analysis determined a moment rate function to calculate GPS measurements from tremor data. We used their moment-rate of 5.17 x $10^{16}$ N-m per hour of tremor to analyze the spatial relationship between tremor and slip.

We examined GPS data to resolve the location of the slip component of ETS events. First, we determined accurate displacements for each GPS station by fitting a hyperbolic tangent function (Figures 7-10) with a fixed slow earthquake duration [*Larson et al*., 2004]. Figures 7-10 are examples of the hyperbolic tangent fit for several stations during each ETS event analyzed (refer to Figure 6 for station locations). The total offset

calculated by the hyperbolic tangent function provides a more precise measurement of surface displacement from cleaned GPS data. Once the displacement was measured, we inverted them using elastic Green's functions from Okada [1992] to determine the geodetically-inferred slip for each fault patch during each individual event. Laplacian smoothing was applied to decrease sharp strain gradients between polygons on the fault interface [*McCrory et al.*, 2012]. We display our results in two ways. First with velocity vector plots to demonstrate the surface offsets at individual stations during each event (Figures 11-14). These plots display the magnitude of surface displacement along with the modeled slip on the fault interface at the location of GPS stations.

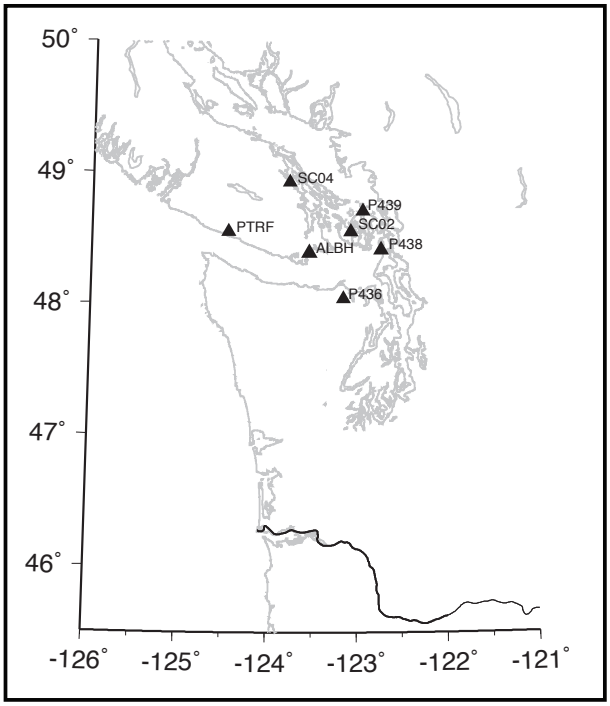


Figure 6: Reference map of northern Cascadia showing the seven GPS stations (black triangles) whose times series appear in subsequent figures.

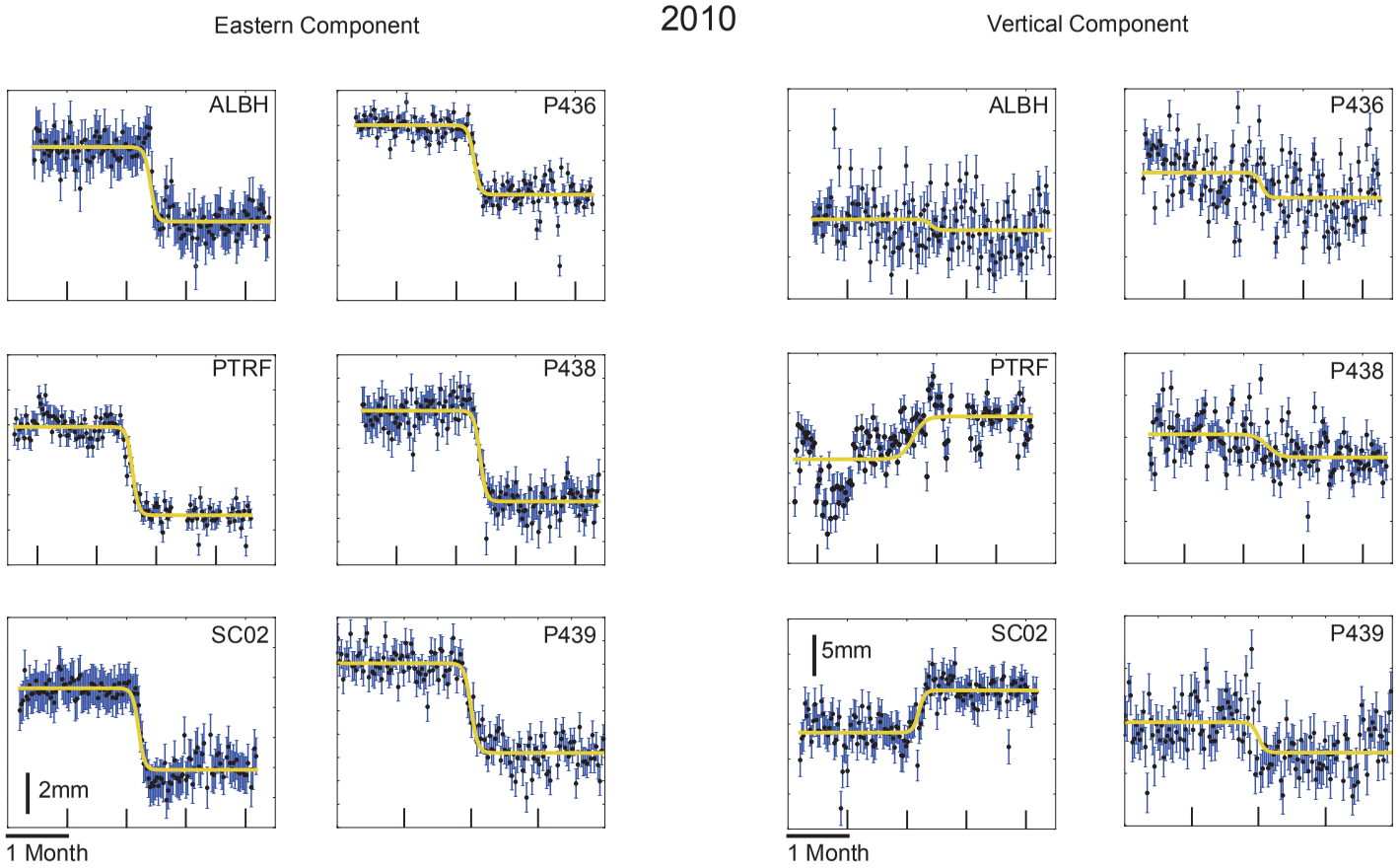


Figure 7: Hyperbolic tangent function fit for 2010 in the east and vertical components. Black dots represent daily position with blue error bars. Yellow line corresponds with the hyperbolic tangent fit for each station with a window of approximately 4 months. The start date for each graph is August 15, 2010. Refer to Figure 6 for the location of GPS stations.

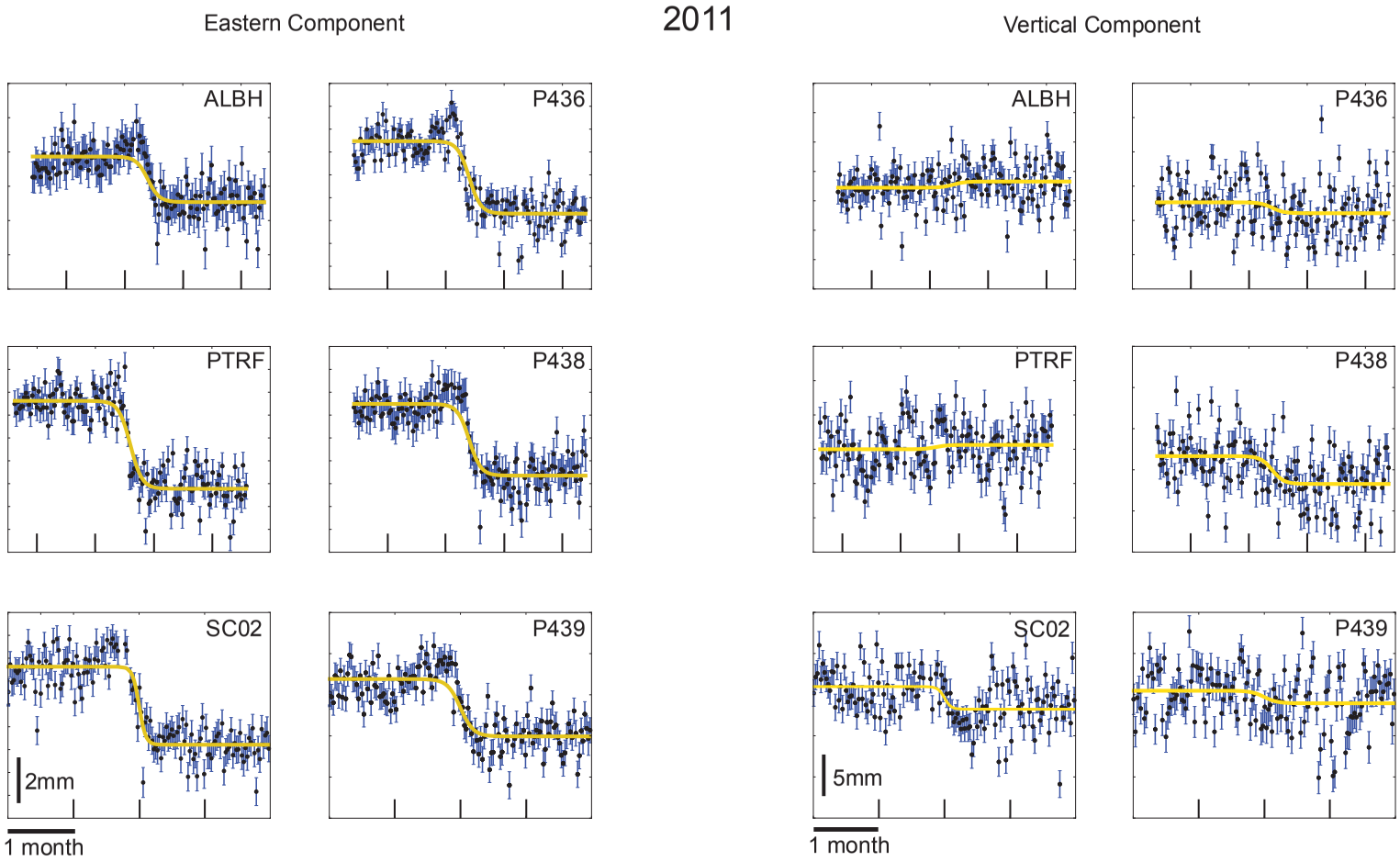


Figure 8: Hyperbolic tangent function fit for 2011 in the eastern and vertical components. Black dots represent daily position with blue error bars. Yellow line corresponds with the hyperbolic tangent fit for each station with a window of approximately 4 months. The start date for each graph is August 15, 2011. Refer to Figure 6 for the location of GPS stations.

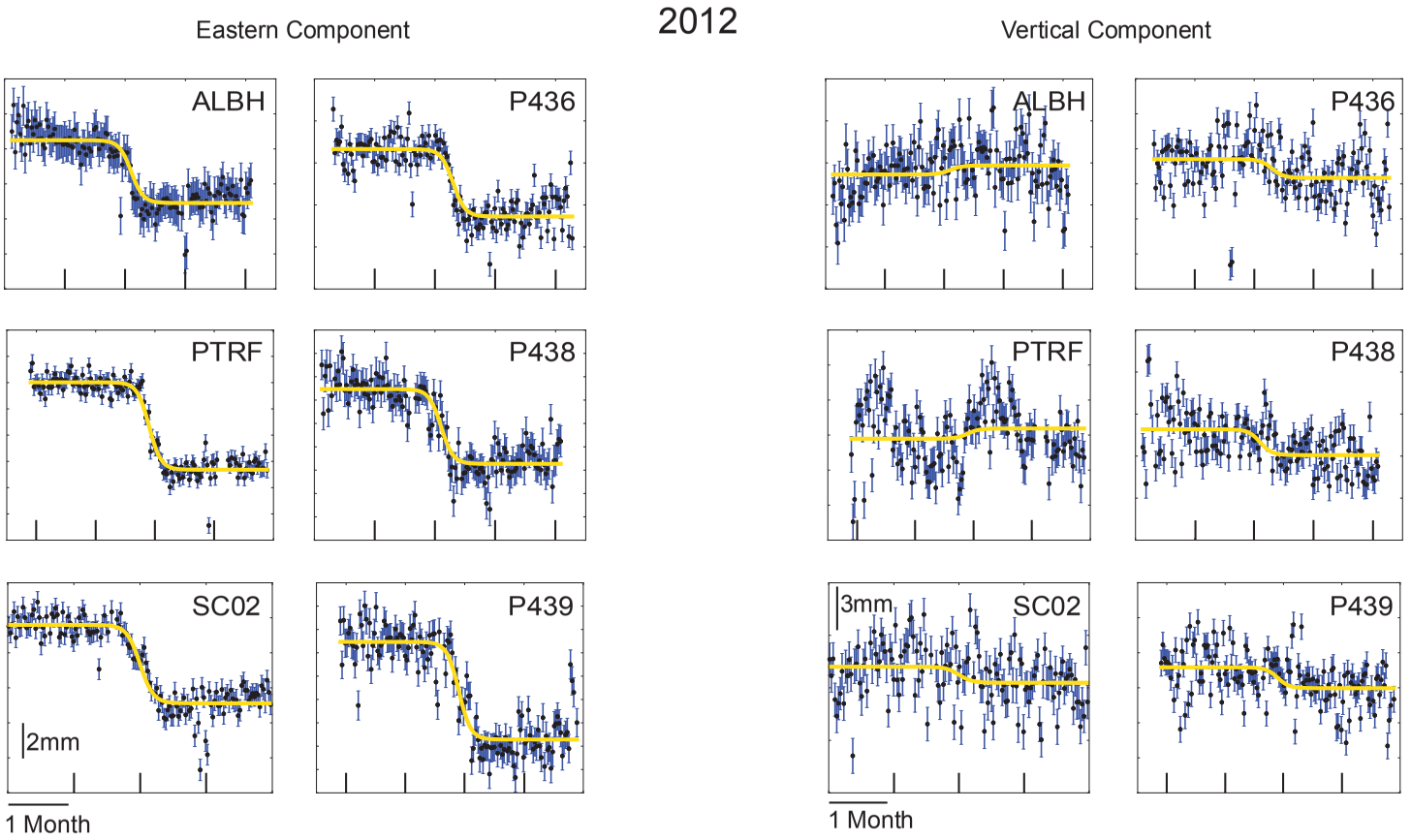


Figure 9: Hyperbolic tangent function fit for 2012 in the east and vertical components. Black dots represent daily position with blue error bars. Yellow line corresponds with the hyperbolic tangent fit for each station with a window of approximately 4 months. The start date for each graph is June 10, 2012. Refer to Figure 6 for the location of GPS stations.

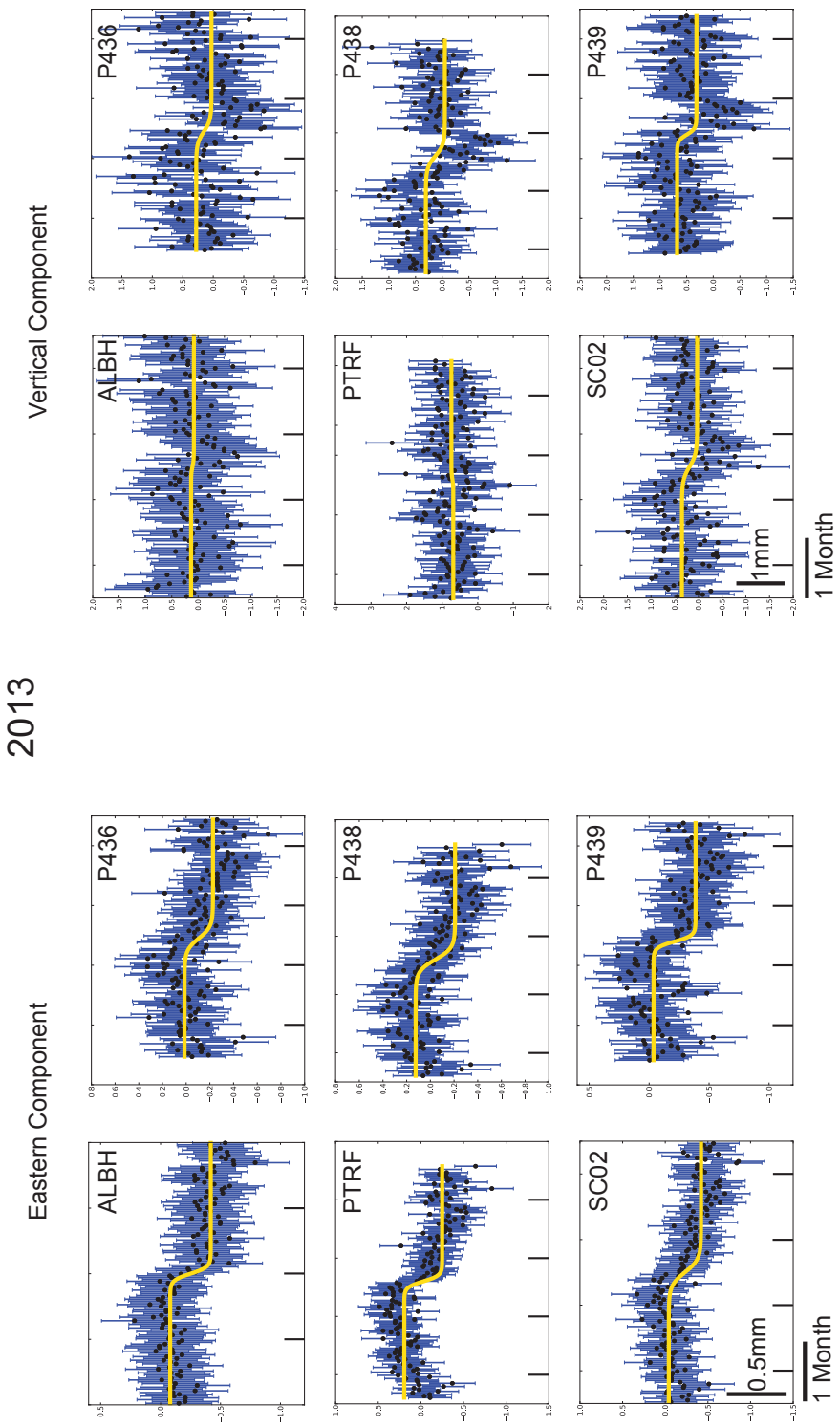


Figure 10: Hyperbolic tangent function fit for 2010 in the east and vertical components. Black dots represent daily position with blue error bars. Yellow line corresponds with the hyperbolic tangent fit for each station with a window of approximately 4 months. The start date for each graph is July 5, 2013. Refer to Figure 6 for the location of GPS stations.

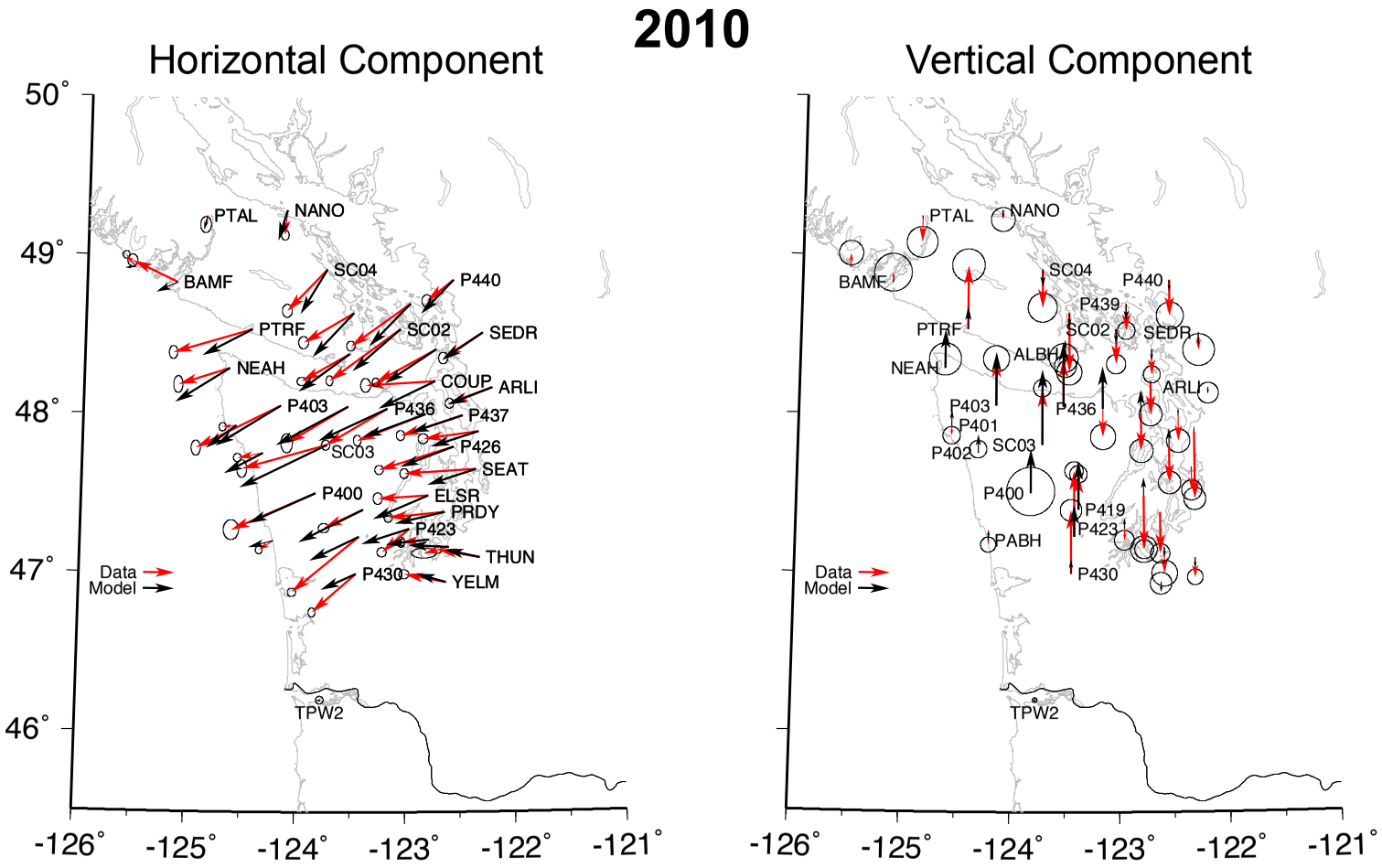


Figure 11: Slow earthquake displacements (red arrows) during the 2010 ETS event and modeled displacements vectors (black) from continuous GPS data. Nearly all of the surface displacements occurred within the northeastern region of the Olympic Peninsula during the 2010 event.

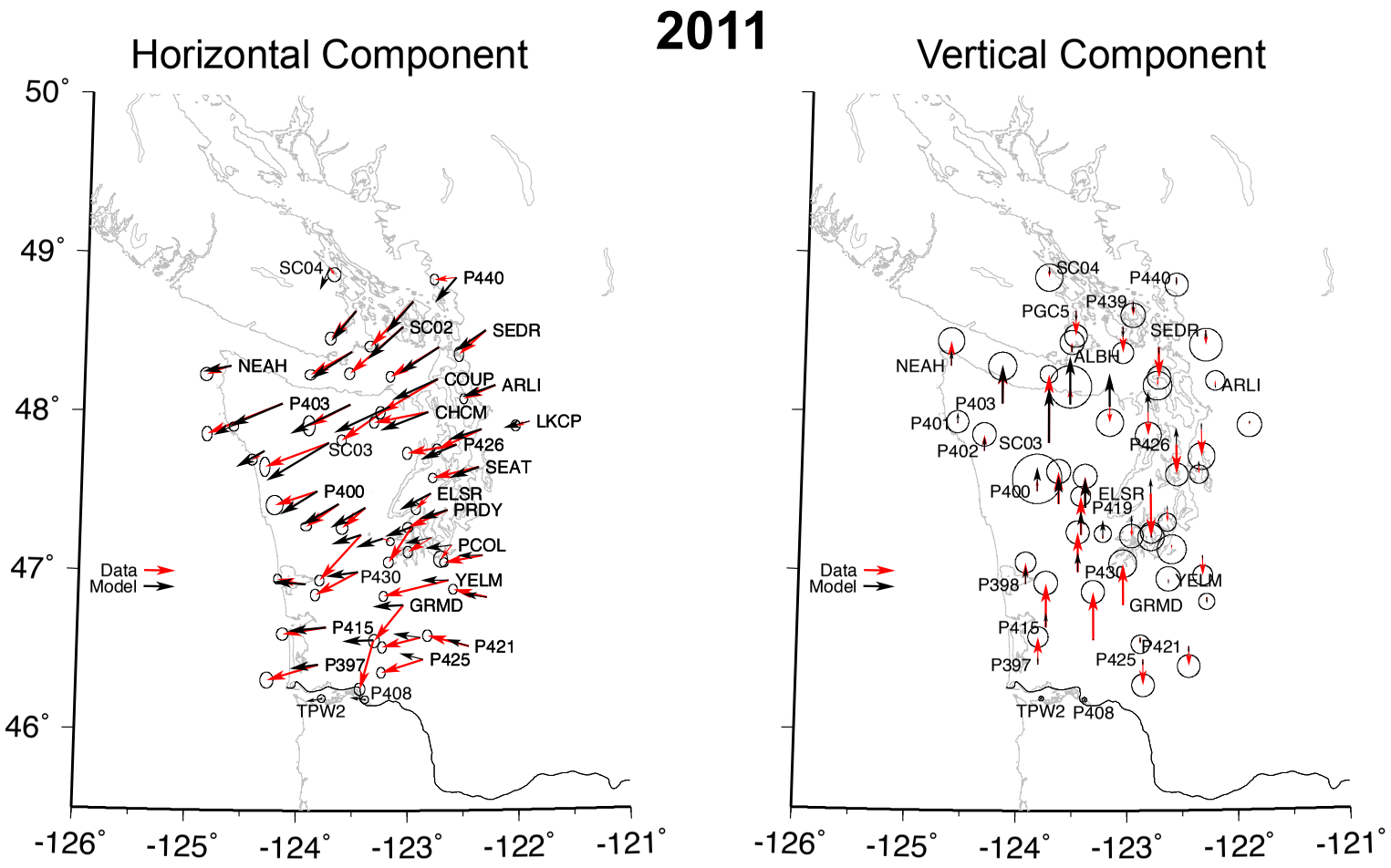


Figure 12: Slow earthquake displacements (red arrows) during the 2011 ETS event and modeled displacements vectors (black) from continuous GPS data. Nearly all of the surface displacements occurred within the northeastern region of the Olympic Peninsula during the 2011 event.

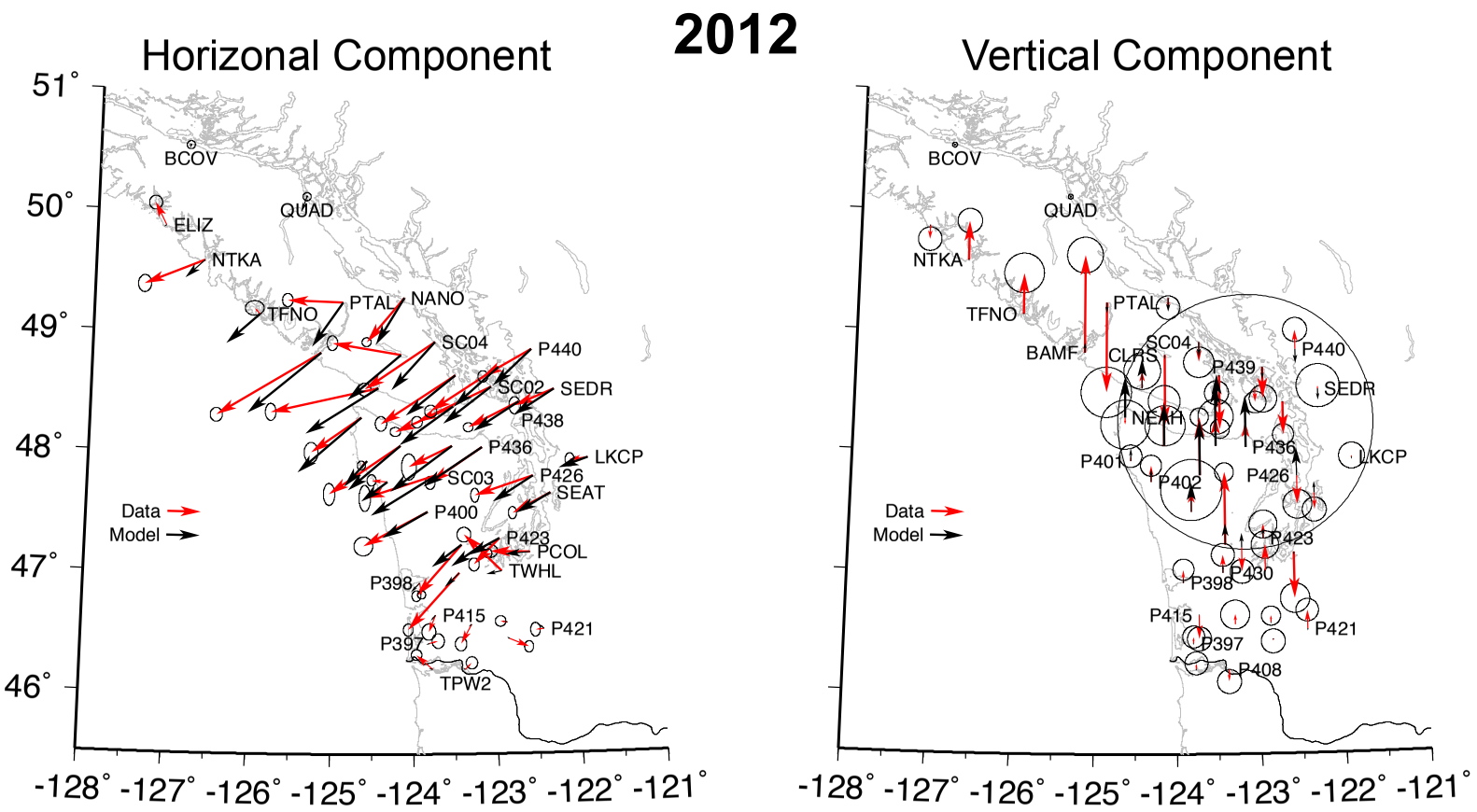


Figure 13: Slow earthquake displacements (red arrows) during the 2012 ETS event and modeled displacements vectors (black) from continuous GPS data. Nearly all of the surface displacements occurred further north of the 2010 or 2011 events, mostly located within the Straits of Juan de Fuca and under Vancouver Island, B.C. during the 2012 event.

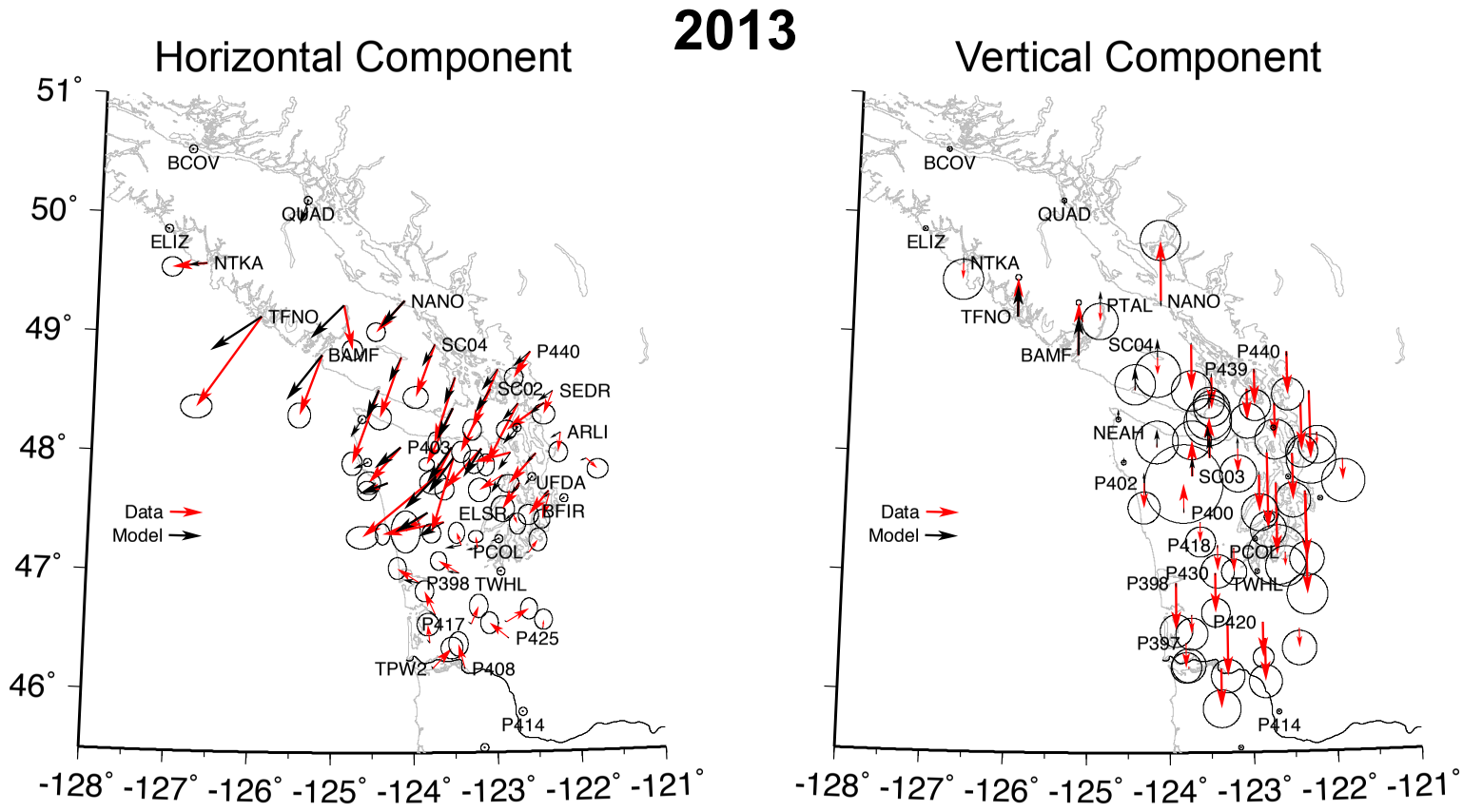


Figure 14: Slow earthquake displacements (red arrows) during the 2013 ETS event and modeled displacements vectors (black) from continuous GPS data. The surface displacements occurred in relatively the same region as the 2012 ETS event; just north of the Olympic Peninsula, into Vancouver Island, B.C

and our modeled interpretation of the amount of slip on the fault interface determined by our inversion. We also created slip distribution maps (Figure 15) from the calculated inferred slip and plot the results on a parameterized plate interface of the Cascadia subduction zone. The slip distribution maps provide the estimated location of the slip on the fault interface during ETS events.

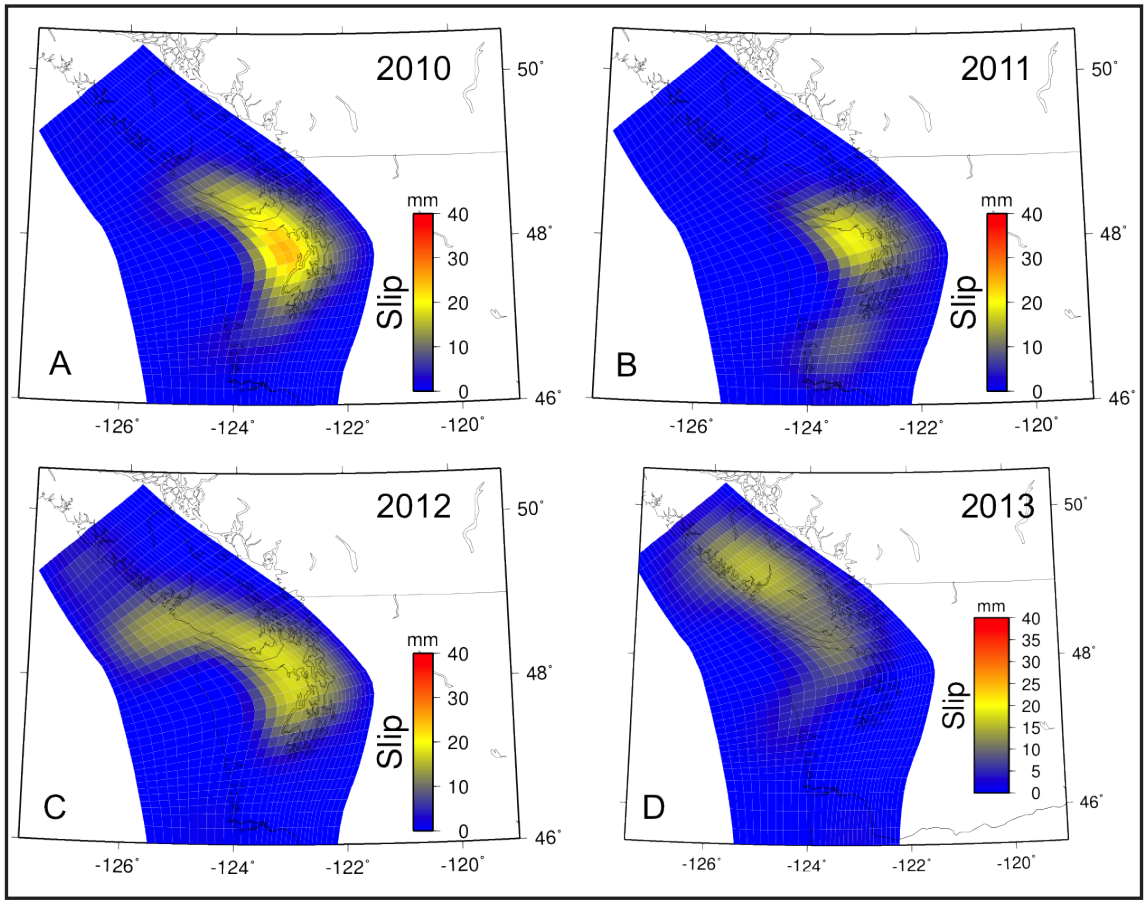


Figure 15: Slip distributions for each of the 4 ETS events occurring during the period 2010–2013 in northern Cascadia. Slip on the plate interface is modeled from GPS observations of surface deformation shown in Figures 11-14. The majority of the slip occurs at approximately 30 km depth. The shape and depth of the plate interface is from McCrory et al., 2012.

We analyzed tremor location and duration data [*Wech*, 2010] by applying a linear moment-rate function [*Aguiar et al.*, 2009] to convert tremor data to predicted GPS

measurements. This data set contained tremor burst locations and durations in 5-minute increments. For each burst of tremor, there was a 2.5-minute (50%) overlap to ensure there was no missing data. We then assumed linear scaling between seismic tremor and moment [*Ide et al.*, 2007; *Aguiar et al.*, 2009]. Since depth information for tremor bursts is poor, we assumed that each tremor burst is located directly below its epicentral location and on the plate interface. Once the data was projected onto the fault interface below the epicentral locations, we forward modeled the tremor as a dislocation to predict GPS measurements. We re-ran this procedure with different distances, up-dip and down-dip, along the fault interface from their original locations, and calculated the expected surface displacement signals at each GPS station. We find that the tremor locations must be moved up-dip along the fault interface by roughly 15 km to match the expected GPS offsets shape and relative amplitude (Figure 16).

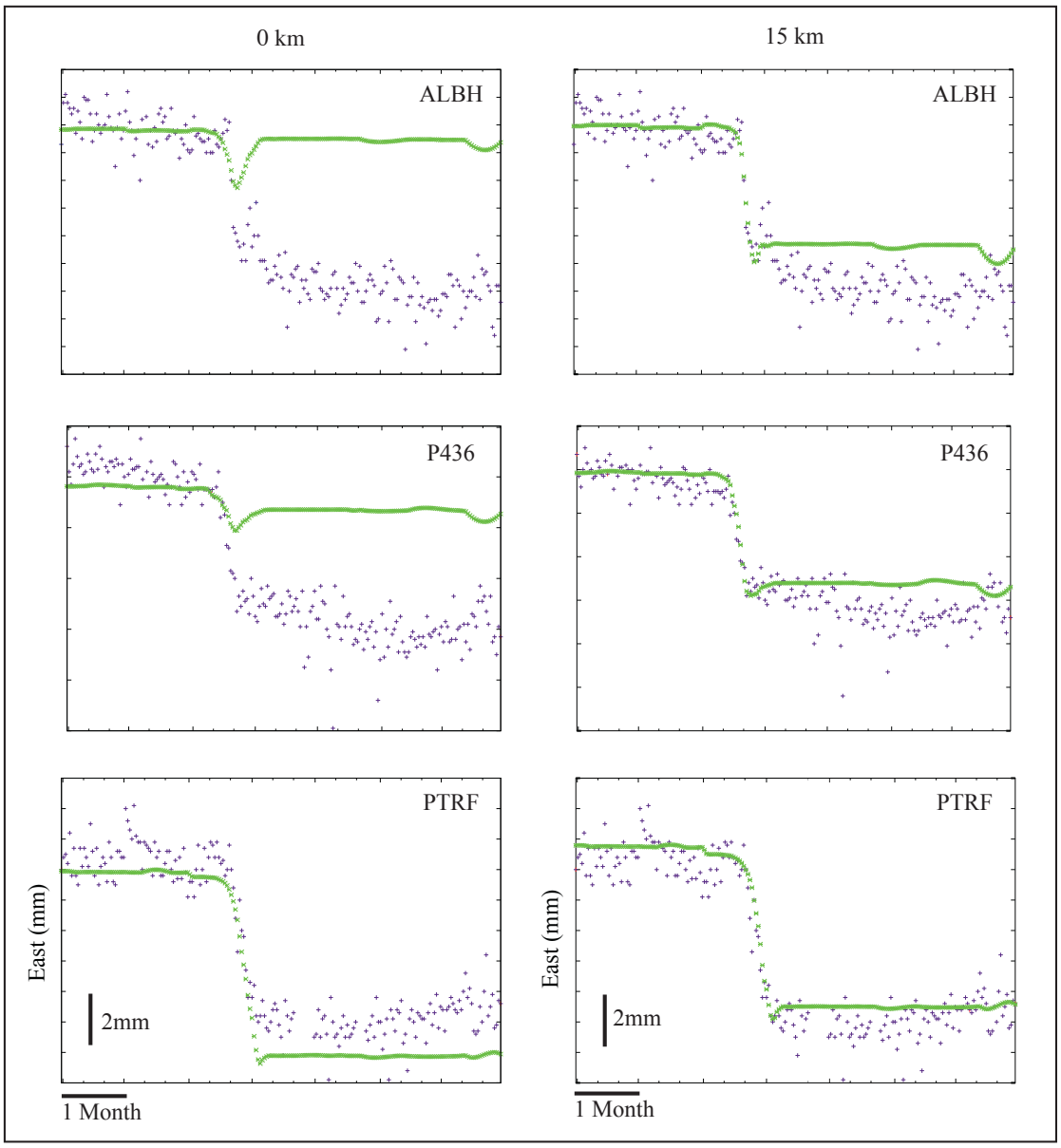


Figure 16: Comparison of synthetic GPS data (green) predicted from tremor burst data with actual daily GPS observations (purple). Left column shows tremor bursts located on the plate interface directly below the epicentral locations calculated by the PNSN. The right column shows the same tremor bursts moved 15 km up-dip from their epicentral locations calculated by the PNSN. All plots begin on August 15, 2010 with a horizontal black bar indicating duration of one month. Y-axis represents eastward displacement in mm with the vertical black bar representing 2 mm.

### 3. FastICA application

Typical earthquake location algorithms rely on the clear distinction of P- and S-wave arrivals and the difference between P- and S-wave velocities in the solid Earth. The emergent nature of non-volcanic tremor (Figure 17) coupled with a near-complete lack of identifiable phases [*Obara*, 2002; *Dragert et al*., 2004] render these traditional algorithms useless. Thus, location strategies for non-volcanic tremor have typically involved the cross-correlation of waveform envelopes [*Kao and Shan*, 2004, *McCausland et al.*, 2005]. This method hinges on differences in the arrival times of high amplitude tremor bursts on different stations rather than differences in the arrival times of coherent phases with known travel times. Thus, the accuracy of locations derived from envelope cross-correlation are unknown due to uncertainty in the travel times of individual tremor bursts.

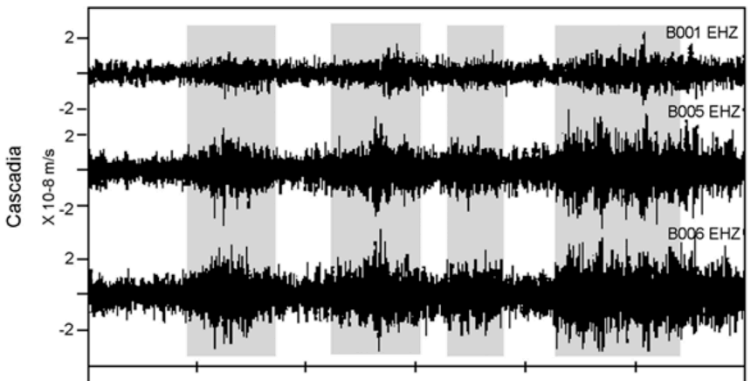


Figure 17: Example of non-volcanic tremor from seismic records in Cascadia. Areas highlighted in gray represent non-volcanic tremor signal. Modified from Aguiar et al., 2009.

Recent investigations, however, have begun to suggest that some non-volcanic tremor waveforms do, in fact, contain recognizable S-wave and occasional P-wave arrivals [*Shelly et al.*, 2006]. The possibility that non-volcanic tremor waveforms consist of typical body-wave arrivals raises the question of why these phases are not often

discernible in the data. One possibility is that non-volcanic tremor signals consists of coherent P and S-wave arrivals from multiple, closely spaced sources, and the observed emergent nature is the result of destructive interference. If one were able to separate out each coherent source, distinct P and S-wave arrivals should be visible. In this way, the identification of these distinct sources becomes analogous to the solution of the cocktail party problem from machine learning [*Haykin and Chen*, 2005].

Strategies for solving the cocktail party problem have been investigated in the past decade [*Haykin and Chen*, 2005]. This process is analogous to several microphones in a room hosting a cocktail party. The microphones are recording the guests as they converse. Each guests voice has its own unique waveform signature that is later separated from the cluster of voices on the recording by employing a FastICA application. Common strategies used to resolve this problem involve two primary methodologies, and employ either Independent Component Analysis (ICA) or Principal Component Analysis (PCA). PCA methods seek to separate input signals into orthogonal bases, or uncorrelated variables. By comparison, ICA separates a signal into statistically independent variables. These two approaches are distinct because statistical independence implies non-correlation, but non-correlation does not imply statistical independence.

Calculation of the components in PCA relies on second-order statistical moments (e.g. variance) and, as such, depends on Gaussian components. Calculation of the components in ICA relies on higher-order statistical moments and performs much better when non-Gaussian signals are involved [*Comon*, 1994]. Since earthquake phase

arrivals, in particular early arriving body-wave phases have been shown to exhibit non-Gaussian characteristics [*Persson*, 2000], ICA appears to be the preferable algorithm for our task.

We chose the Fast Independent Component Analysis (FastICA) algorithm as our computation algorithm in our attempt to determine statistically unique tremor signals. The FastICA algorithm takes *n* simultaneously recorded signals from additively mixed sources and separates them into, at most, *n* statistically independent signals. Our application of the FastICA attempts to separate the individual tremor signals during tremor bursts.

We attempted to employ the FastICA algorithm to data from a campaign network consisting of eight broadband seismic stations that were installed prior to the 2010 ETS event near Sequim, WA (refer to Figures 1 and 5). These seismic stations recorded several weeks of tremor data that coincided in time with the GPS recorded ETS event. We analyzed sections of data with the strongest tremor and employed the FastICA algorithm, but did not yield clear P- or S-wave arrivals. Issues with signal delay and noise may have made interpretation difficult and our results were inconclusive. Suggestions for future work include creating a trial data set containing mixtures of known individual tremor signals to test whether the FastICA algorithm can reproduce the input set of known tremor signals.

## 4. Results

During our analysis of predicted GPS measurements, we found that the predicted GPS measurements calculated by the tremor had much larger offsets than the actual recorded observations by the GPS stations. In order to compensate for the larger displacements we scaled the moment rate function from Aguiar et al. [2009] by a factor of roughly 0.5. In order to best fit the observed geodetic slip signals, scaling factors were varied station-by-station and event-to-event. The average scaling factors were 0.48, 0.45, 0.46, and 0.60 for the 2010, 2011, 2012, and 2013 events respectively (Figures 1920). We conclude that on average, the moment rate function used in the Aguiar et al. [2009] study must be reduced by roughly half in order to best match observed geodetic data. We consider the amount of tremor that is recorded by seismic stations has increased drastically due to the number of stations installed since their study. Since there are approximately 125 seismic stations located within the originating location of tremor, near Puget Sound, seismic tremor may be recorded for a longer duration as compared with previous slow earthquakes. This would lead to an increase in observed tremor and may be a viable explanation as to why the predicted GPS measurements had much larger offsets.

By comparing the location of tremor and slip in map view (Figure 18), it is difficult to decipher whether they are produced from the same location on the fault interface. We are able to confidently determine the location of slip by inverting GPS displacement measurements. This results in slip centered at approximately 30 km depth, on the fault interface (Figure 15). However, in order to reproduce the shape of GPS

surface displacement observations, it was necessary to move tremor locations up-dip 15 km (Figure 16). This strong agreement in time series shape suggests tight temporal correlation of tremor and slip. However, the requirement of relocating the tremor suggests close, but imperfect, co-location. These features are not apparent when considering the gross locations from both methods (Figure 18).

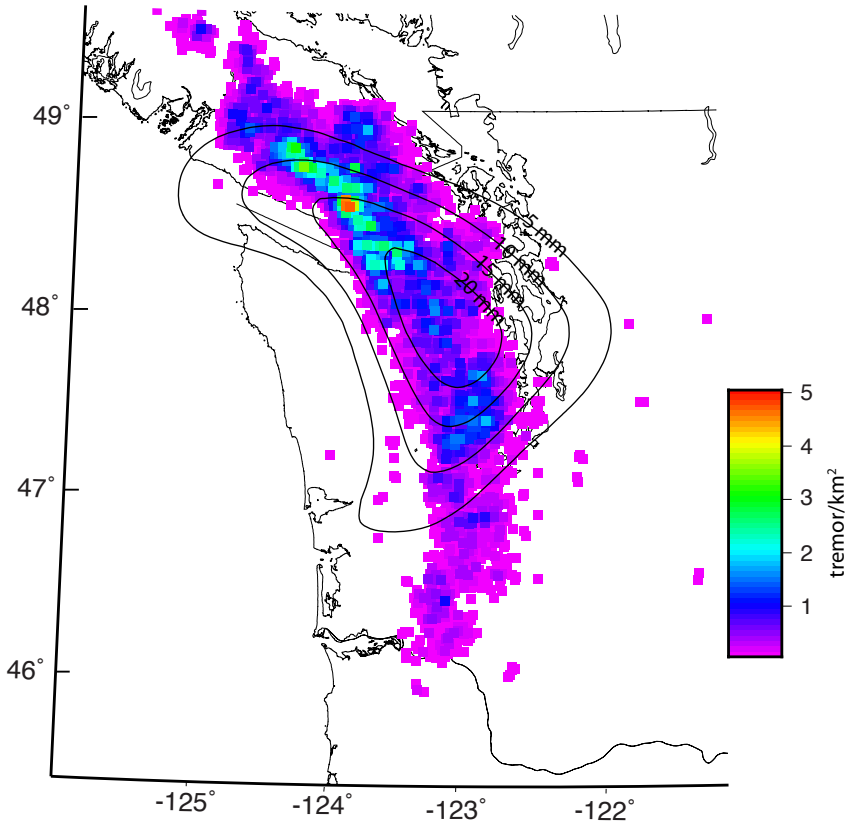


Figure 18: GPS inferred slip (contours) and seismically observed tremor density (colored squares) for the 2010 ETS. Note the broad overlap of both aspects of ETS. Tremor density is represented as a count of total number of tremor events per square km. Slip is the same as in Figure 15. Maximum slip for this ETS event is 24 mm.

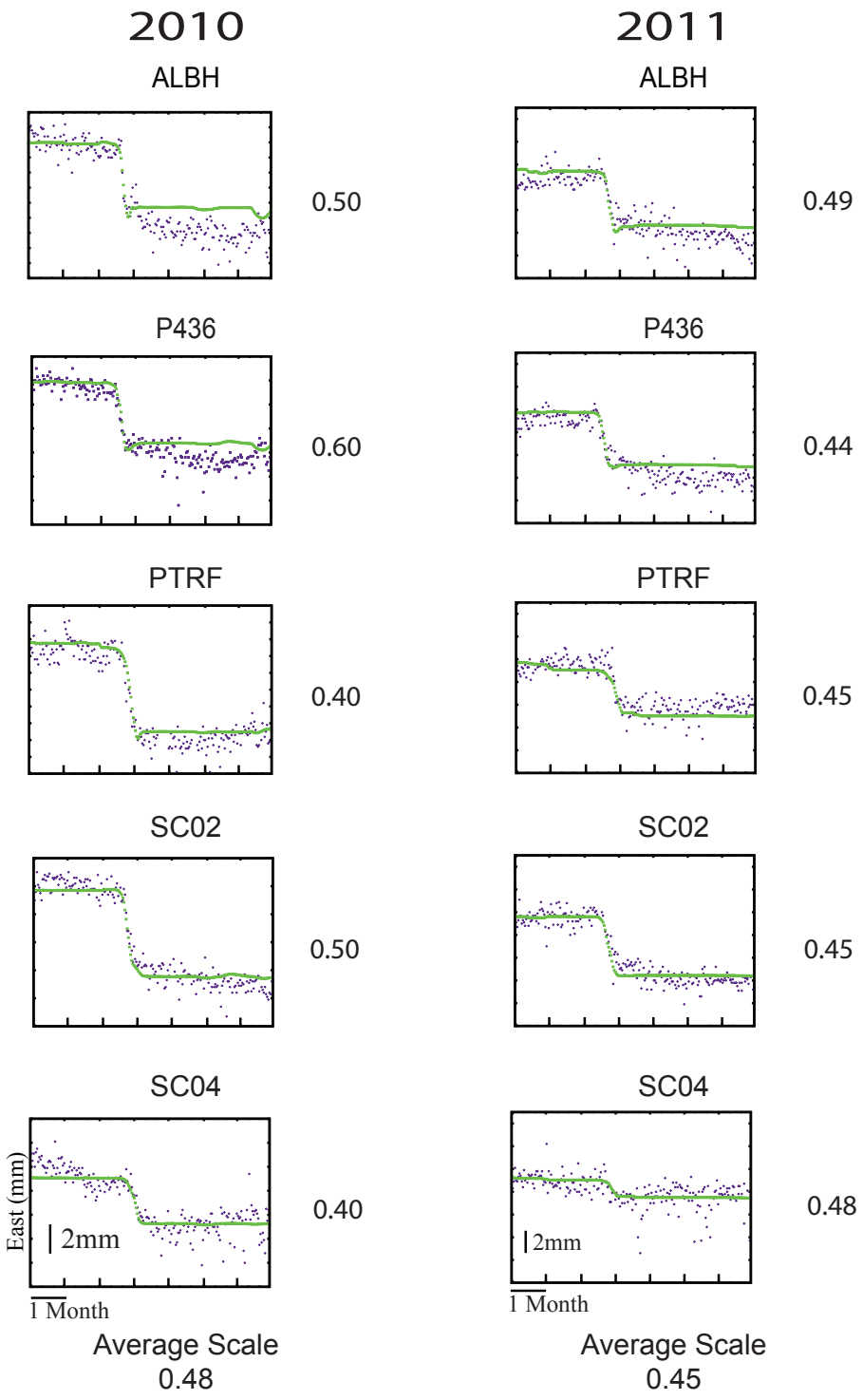


Figure 19: Fit of synthetic GPS (green) from tremor data with respect to measured GPS data (purple) for 2010–2011 ETS events. The synthetic GPS is calculated at 15 km up-dip of epicentral locations projected on the fault interface. Numbers to the right of each plot indicate the required scaling of the synthetic GPS to fit the measured GPS signal. All plots begin on June 1, 2010 and 2011 respectively with a horizontal bar indicating a duration of one month. Y-axis represents eastward displacement in mm with the vertical black bar representing 2 mm.

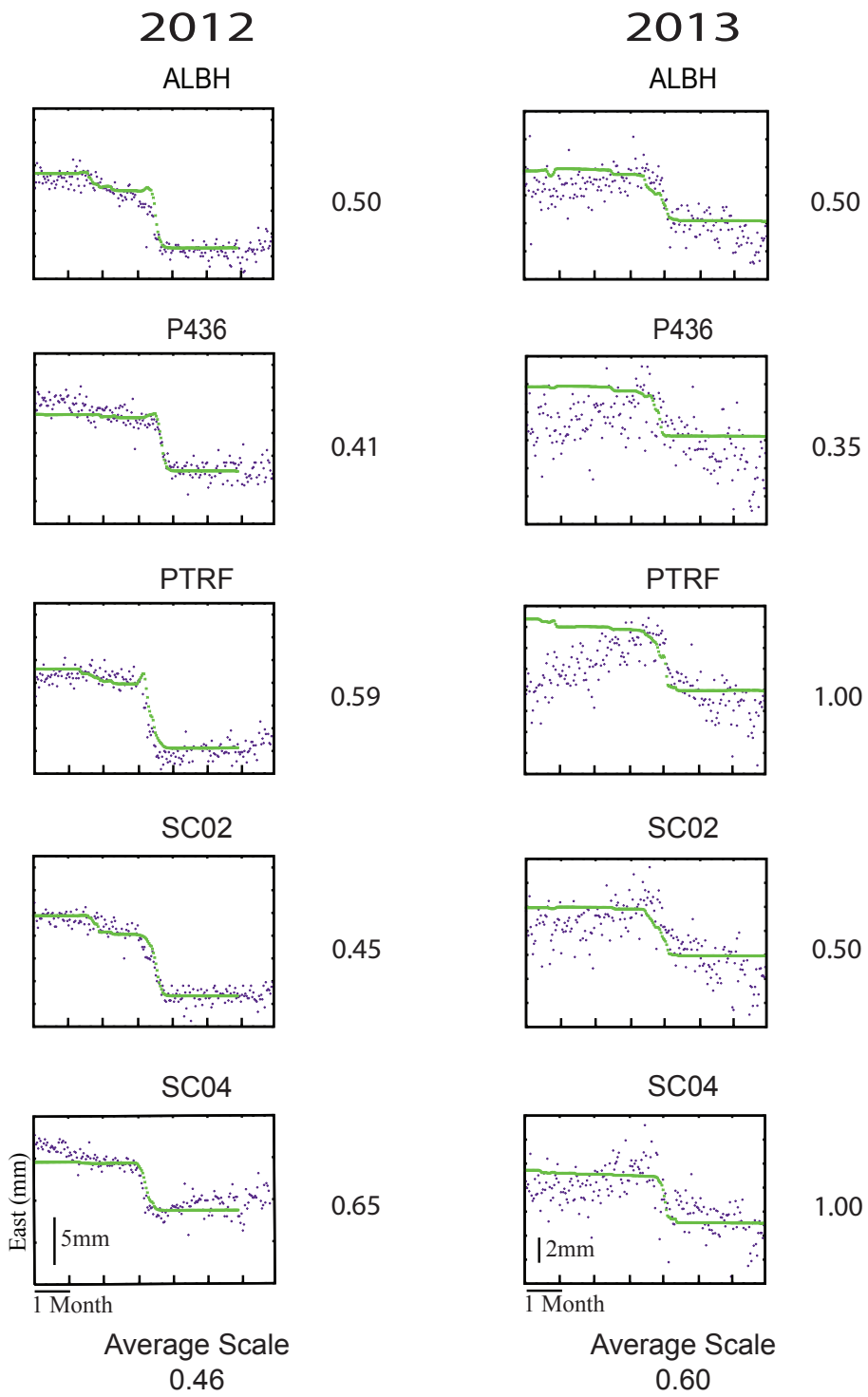


Figure 20: Fit of synthetic GPS (green) from tremor data with respect to measured GPS data (purple) for 2012–2013 ETS events. The synthetic GPS is calculated at 15 km up-dip of epicentral locations projected on the fault interface. Numbers to the right of each plot indicate the required scaling of the synthetic GPS to fit the measured GPS signal. All plots begin on June 1, 2012 and 2013 respectively with a horizontal bar indicating a duration of one month. Y-axis represents eastward displacement in mm with the vertical black bar representing 5 and 2 mm, respectively.

**5. Discussion and conclusions of spatial relationship**

Geodetically-inferred slip and seismic tremor occur contemporaneously during ETS events and are thought to be two manifestations of the same process [*Rogers and Dragert*, 2003; *Obara et al.*, 2004]. GPS networks, such as PANGA and MEASURES, and the seismic array PNSN captured data representing these two aspects during ETS events occurring in 2010–2013. Results from our study show that slip and tremor occur synchronously but are spatially separate processes because the timing of the events are comparable, however, PNSN tremor locations appear deeper on the plate interface than slip due to the need to move these locations up-dip to reproduce GPS surface observations. This aspect of ETS cannot be easily seen by plotting bulk tremor and slip locations (Figure 18).

Inverting GPS data resulted in moment magnitudes of between $M_W$ 6.7-6.8 for each of the 2010, 2011, 2012, and 2013 ETS events studied. The slip distribution for each event show the majority of slip occurring at approximately 30 km depth on the fault interface similar to previous work [*Szeliga et al.*, 2004; *Szeliga et al.*, 2008]. The 2010 ETS event had the most localized slip distribution, centered about the northeastern Olympic Peninsula, WA at a depth of approximately 30 km. The 2011 event is well constrained near the same region as the 2010 event, however, a very small amount of slip is projected toward southwestern Washington. This is believed to be due to remnant signals from another ETS event occurring farther south on the CSZ. The 2012 event is relatively well constrained in the northeastern portion of the Olympic Peninsula but has recorded GPS displacements farther north along Vancouver Island, BC. Since there are

no GPS stations located off shore, the slip cannot be constrained to an acceptable up-dip depth and is an artifact of the model. The 2013 event had the least constrained slip distribution. This is due to the lack of data available; since most of the slip occurred below Vancouver Island, B.C., the stations that recorded the surface deformation were limited.

Tremor during these events, however, is suggested to occur below the slip on the fault interface. This is suggested by the necessity of moving tremor locations up-dip 15 km in order to reproduce GPS surface observations (Figures 16, 19, and 20). When we compared our predicted GPS from tremor data to the actual GPS measurements and determine that it was essential for the moment rate function calculated by Aguiar et al. [2009] to be scaled by approximately 0.5. A possible reason for scaling the moment rate function was because of the substantial amount of instruments added to the network. The increase in instrumentation available to record data provided a significant increase in the amount of tremor recorded. Each station was analyzed and scaled appropriately. We then averaged the scaling factors for each year to determine an average scaling factor; which are as follows: 0.48, 0.45, 0.46, and 0.60 for the 2010, 2011, 2012, and 2013 ETS events respectively (Figures 19 and 20). All of these results suggest that tremor and slip do occur simultaneously in time but are spatially separate phenomena.

Although we attempted to employ the FastICA algorithm to determine statistically independent tremor signals, our results were inconclusive. Locating tremor is a difficult task due to the lack of depth resolution from seismic records. Since tremor signals lack impulsive P- and S-waveforms, calculating the location of tremor at depth is nearly

impossible. The presence of P- and S- waveforms would allow for the calculation of accurate tremor locations, including tremor depth, using standard seismological algorithms. We employed the FastICA algorithm in an attempt to extract these waveforms from the data. We were unable to recover coherent P- or S-waveforms. It is unclear whether signal delay or noise may have been factors leading to incoherent waveforms.

# REFERENCES

## JOURNAL REFERENCES

Adams, J. (1990), Paleoseismicity of the Cascadia subduction zone: evidence from turbidites off the Oregon-Washington margin, *Tectonics*, 9(4), 569-583.

Aguiar, A. C., T. I. Melbourne, and C. W. Scrivner (2009), Moment release rate for Cascadia tremor constrained by GPS, *J. Geophys. Res.*, 114(B00A05), doi:10.1029/2008JB005909.

Atwater, B. F (1992), Geologic evidence for earthquakes during the past 2000 years along the Copalis River, southern coastal Washington, *J. Geophys. Res.*, 97(B2), 1901–1919.

Atwater, B. F., and Hemphill-Haley, *Recurrence intervals for great earthquakes of the past 3,500 years at northeastern Willapa Bay, Washington*, USGS Professional Paper: 1576, U.S. G.P.O, 1997.

Beroza, G. C., and S. Ide (2011), Slow earthquakes and nonvolcanic tremor, *Annu. Rev. Earth Planet Sci.*, 39, 271-296, doi: 10.1146/annurev-earth-040809-152531.

Comon, P. (1994), Independent component analysis, a new concept?, *Signal Processing*, 36(3), 287-314, doi:10.1016/0165-1684(94)90029-9.

Creager, K. C. and T. I. Melbourne (2007), Episodic tremor and slip in the Pacific Northwest, *Earth Scope onSite Newsletter*, 1-3.

Dragert, H., K. Wang, and T. S. James (2001), A silent slip event on the deeper Cascadia subduction interface, *Science,* 292(5521), 1525-1528.

Dragert, H., K. Wang, and G. Rogers (2004), Geodetic and seismic signatures of episodic tremor and slip in the northern Cascadia subduction zone, *Earth, Planets, and Space* 56, 1143-1150.

Flück, P., R. D. Hyndman, and K. Wang (1997), Three-dimensional dislocation model for great earthquakes of the Cascadia subduction zone, *J. Geophys. Res.*, *102*(B9), 20,359–20,550, doi:10.1029/97JB01642.

Goldfinger, C., C. H. Nelson, and J. E. Johnson (2003), Holocene earthquake records from the Cascadia subduction zone and northern San Andreas fault based on precise dating of offshore turbities, *Ann. Rev. Earth Planet Sci.*, 31, 555-577, doi: 10.1146/annurev.earth31.100901.141246.

Haykin, S., and Z. Chen (2005), The cocktail party problem, *Neural computation*, 17(9), 1875-1902.

Ide, S., G. C. Beroza, D. R. Shelly, and T. Uchide (2007), A scaling law for slow earthquakes, *Nature*, 447, 76-79, doi:10.1038/nature05780.

Ito, Y., et al. (2012), Episodic slow slip events in the Japan subduction zone before the 2011 Tohoku-Oki earthquake, *Tectonophysics*, doi:10.1016/j.tecto.2012.08.022.

Kao, H., and S. Shan (2004), The source-scanning algorithm: Mapping the distribution of seismic sources in time and space, *Geophysical Journal International*, 157(2), 589-594.

Kao, H., S. Shan, H. Dragert, and G. Rogers (2009), Northern Cascadia episodic tremor and slip: a decade of tremor observations from 1997 to 2007, *J. Geophys Res.*, 114.B11 (2009), doi:10.1029/2008JB/006046.

Larson, K. M., A. R. Lowry, V. Kostoglodov, W. Hutton, O. Sánchez, K. Hudnut, and G. Suárez (2004), Crustal deformation measurements in Guerrero, Mexico, *J. Geophys. Res.*, 109(B4), doi:10.1029/2003JB002843.

McCausland, W., S. Malone, and D. Johnson (2005), Temporal and spatial occurrence of deep non-volcanic tremor: From Washington to northern California, *Geophysical Research Letters*, 32(24), doi:10.1029/2005GL024349.

McCrory, P. A., J. L. Blair, F. Waldhauser, and D. H. Oppenheimer (2012), Juan de Fuca slab geometry and its relation to Wadati-Benioff zone seismicity, *J. Geophys. Res.*, *117*(B09306), doi:10.1029/2012JB009407.

Melbourne, T. I., and F. H. Webb (2003), Slow but not quite silent, *Science*, 300, 1886-1887.

Melbourne, T. I., W. M. Szeliga, M. M. Miller, and V. M. Santillan (2005), Extent and duration of the 2003 Cascadia slow earthquake, *Geophysical Research Letters* 32(4), doi:10.1029/2004GL021790.

Miller, M. M., T. I. Melbourne, D. J. Johnson, and W. Q. Sumner (2002), Periodic Slow Earthquakes from the Cascadia Subduction Zone, *Science*, *295*(5564), 2423.

Obara, K. (2002), Nonvolcanic deep tremor associated with subduction in southwest Japan, *Science*, 296, 1679-1681.

Obara, K., H. Hirose, F. Yamamizu, and K. Kasahara (2004), Episodic slow slip events accompanied by non-volcanic tremors in southwest Japan subduction zone, *Geophysical Research Letters*, 31(23), doi:10.1029/2004GL020848.

Okada, Y. (1992), Internal deformation due to shear and tensile faults in a half-space, *Bulletin of the Seismological Society of America*, *82*(2), 1018–1040.

Persson, L. 2003, Statistical tests for regional seismic phase characterizations, *Journal of Seismology*, 7(1), 19-33.

Rogers, G. (2007, April). Episodic Tremor and Slip in Northern Cascadia–Going Back in Time, paper presented at the 2007 Seismol. Soc. Am. In *Annual Meeting, Waikoloa, Hawaii*, 11-13.

Rogers, G., and H. Dragert (2003), Episodic tremor and slip on the Cascadia subduction zone: The chatter of silent slip, *Science*, 300(5627) 1942-1943.

Rubinstein, J. L., J. Gomberg, J. E. Vidale, A. G. Wech, H. Kao, K. C. Creager, and G. Rogers (2009), Seismic wave triggering of nonvolcanic tremor, episodic tremor and slip, and earthquakes on Vancouver Island, *J. Geophys. Res.*, 114(B2), doi:10.1029/2008JB005875.

Satake, K., K. Wang, and B. F. Atwater (2003), Fault slip and seismic moment of the 1700 Cascadia earthquake inferred from Japanese tsunami descriptions, *J. Geophys. Res.*, 108(11), doi:10.1029/2003JB002521.

Segall, P., A. M. Rubin, A. M. Bradley, and J. R. Rice (2010), Dilatant strengthening as a mechanism for slow slip events, *J. Geophys. Res.,* 115.B12305, doi:10.1029/2010JB007449.

Shelly, D. R., G. C. Beroza, S. Ide, and S. Nakamula (2006), Low-frequency earthquakes in Shikoku, Japan, and their relationship to episodic tremor and slip, *Nature* 442, 188-191, doi:10.1038/nature04931.

Szeliga, W. M., T. M. Melbourne, M. M. Miller, and V. M. Santillan (2004), Southern Cascadia episodic slow earthquakes, *J. Geophys. Res.*, 31(L16602), doi:10.1029/2004GL020824.

Szeliga, W., T. Melbourne, V. Sanatillan, and M. Miller (2008), GPS constraints on 34 slow slip events within the Cascadia subduction zone, 1997–2005, *J. Geophys. Res.*, 113(B04404), doi:10.1029/2007JB004948.

Wech, A. G. (2010), Interactive tremor monitoring, *Seismological Research Letters*, 81(4), 664-669, doi:10.1785/gssrl.81.4.664.

Wech, A. G., and K. C. Creager (2007), Cascadia tremor polarization evidence for plate interface slip, *Geophysical Research Letters*, 34(22), doi:10.1029/2007GL031167.

Wech, A. G., and K. C. Creager (2008), Automated detection and location of Cascadia tremor, *Geophysical Research Letters*, 35(20), doi:10.1029/2008GL035458.

Wech, A. G., K. C. Creager, and T. I. Melbourne (2009), Seismic and geodetic constraints on Cascadia slow slip, *J. Geophys. Res.*, 114(B10), doi:10.1029/2008JB006090.

Witter, R. C., H. M. Kelsey, and E. Hemphill-Haley (2003), Great Cascadia earthquakes and tsunamis of the past 6700 years, Coquille River estuary, southern coastal Oregon, *GSA Bull.*, 115(10), 1289-1306, doi: 10.1130/B25189.1.

## COMPREHENSIVE REFERENCES

Adams, J. (1990), Paleoseismicity of the Cascadia subduction zone: evidence from turbidites off the Oregon-Washington margin, *Tectonics*, 9(4), 569-583.

Aguiar, A. C., T. I. Melbourne, and C. W. Scrivner (2009), Moment release rate for Cascadia tremor constrained by GPS, *J. Geophys. Res.*, 114(B00A05), doi:10.1029/2008JB005909.

Atwater, B. F. (1987), Evidence for great Holocene earthquakes along the outer coast of Washington state, *Science*, 236(4804), 942-944.

Atwater, B. F., and Hemphill-Haley (1997), Recurrence intervals for great earthquakes of the past 3,500 years at northeastern Willapa Bay, Washington, USGS Professional Paper: 1576, U.S. G.P.O.

Atwater, B. F., M. R. Satoko, S. Kenji, T. Yoshinobu, U. Kazue, and D. K. Yamaguchi (2005). The Orphan Tsunami of 1700: Japanese Clues to a Parent Earthquake in North America. Seattle: University of Washington Press.

Beroza, G. C., and S. Ide (2011), Slow earthquakes and nonvolcanic tremor, *Annu. Rev. Earth Planet Sci.*, 39, 271-296, doi: 10.1146/annurev-earth-040809-152531.

Chapman, J. S., and T. I. Melbourne (2009), Future Cascadia megathrust rupture delineated by episodic tremor and slip, *Geophysical Research Letters*, 36(L22301), doi:10.1029/2009GL040465.

Comon, P. (1994), Independent component analysis, a new concept?, *Signal Processing*, 36(3), 287-314, doi:10.1016/0165-1684(94)90029-9.

Creager, K. C. and T. I. Melbourne (2007), Episodic tremor and slip in the Pacific Northwest, *Earth Scope onSite Newsletter*, 1-3.

Dragert, H., K. Wang, and T. S. James (2001), A silent slip event on the deeper Cascadia subduction interface, *Science,* 292(5521), 1525-1528.

Dragert, H., K. Wang, and G. Rogers (2004), Geodetic and seismic signatures of episodic tremor and slip in the northern Cascadia subduction zone, *Earth, Planets, and Space* 56, 1143-1150.

Flück, P., R. D. Hyndman, and K. Wang (1997), Three-dimensional dislocation model for great earthquakes of the Cascadia subduction zone, *J. Geophys. Res.*, *102*(B9), 20,359–20,550, doi:10.1029/97JB01642.

Goldfinger, C., C. H. Nelson, and J. E. Johnson (2003), Holocene earthquake records from the Cascadia subduction zone and northern San Andreas fault based on precise dating of offshore turbities, *Ann. Rev. Earth Planet Sci.*, 31, 555-577, doi: 10.1146/annurev.earth31.100901.141246.

Gomberg, J. (2010), Slow-slip phenomena in Cascadia from 2007 and beyond: A review, *GSA Bulletin*, *122*(7/8), 963–978, doi:10.1130/B30287.1.

Haykin, S., and Z. Chen (2005), The cocktail party problem, *Neural computation*, 17(9), 1875-1902.

Heaton, T. H., and S. H. Hartzell (1987), Earthquake hazards on the Cascadia subduction zone, *Science*, 236, 162-168.

Heaton, T. H., and H. Kanamori (1984), Seismic potential associated with subduction in the northwestern United States, *Bull. Seismol. Soc. Am*., 74(3), 933–941.

Heaton, T. H., and P. D. Snavely, Jr. (1985), Possible tsunami along the northwestern coast of the United States inferred from indian traditions, *Bull. Seismol. Soc. Am.*, 75(5), 1455-1460.

Hyndman, R. D., and K. Wang (1993), Thermal constraints on the zone of major thrust earthquake failure: The Cascadia Subduction Zone, *J. Geophys. Res.*, 98(B2), 2039-2060, doi:10.1029/92JB02279.

Hyvarinen, A. (1999), Fast and robust fixed-point algorithms for independent component analysis, *IEEE Trans. Neutral Networks*, 10(3), 626-634.

Hyvarinen, A., and E. Oja (2000), Independent component analysis: algorithms and applications, *IEEE Trans. Neutral Networks*, 13(4-5), 411-430.

Ide, S., G. C. Beroza, D. R. Shelly, and T. Uchide (2007), A scaling law for slow earthquakes, *Nature*, 447, 76-79, doi:10.1038/nature05780.

Ito, Y., et al. (2012), Episodic slow slip events in the Japan subduction zone before the 2011 Tohoku-Oki earthquake, *Tectonophysics*, doi:10.1016/j.tecto.2012.08.022.

Kao, H., and S. Shan (2004), The source-scanning algorithm: Mapping the distribution of seismic sources in time and space, *Geophysical Journal International*, 157(2), 589-594.

Kao, H., S. Shan, H. Dragert, and G. Rogers (2009), Northern Cascadia episodic tremor and slip: a decade of tremor observations from 1997 to 2007, *J. Geophys Res.*, 114.B11 (2009), doi:10.1029/2008JB/006046.

Larson, K. M., A. R. Lowry, V. Kostoglodov, W. Hutton, O. Sánchez, K. Hudnut, and G. Suárez (2004), Crustal deformation measurements in Guerrero, Mexico, *J. Geophys. Res.*, 109(B4), doi:10.1029/2003JB002843.

McCausland, W., S. Malone, and D. Johnson (2005), Temporal and spatial occurrence of deep non-volcanic tremor: From Washington to northern California, *Geophysical Research Letters*, 32(24), doi:10.1029/2005GL024349.

McCrory, P. A., J. L. Blair, F. Waldhauser, and D. H. Oppenheimer (2012), Juan de Fuca slab geometry and its relation to Wadati-Benioff zone seismicity, *J. Geophys. Res.*, *117*(B09306), doi:10.1029/2012JB009407.

Melbourne, T. I., and F. H. Webb (2003), Slow but not quite silent, *Science*, 300, 1886-1887.

Melbourne, T. I., W. M. Szeliga, M. M. Miller, and V. M. Santillan (2005), Extent and duration of the 2003 Cascadia slow earthquake, *Geophysical Research Letters* 32(4), doi:10.1029/2004GL021790.

Miller, M. M., T. I. Melbourne, D. J. Johnson, and W. Q. Sumner (2002), Periodic Slow Earthquakes from the Cascadia Subduction Zone, *Science*, *295*(5564), 2423.

Nedimović, M. R., R. D. Hyndman, K. Ramachandran, G. D. Spence (2003), Reflection signature of seismic and aseismic slip on the northern Cascadia subduction interface, *Nature*, 424, 416-420, doi:10.1038/nature01840.

Nelson, A. R., H. M. Kelsey, and R. C. Witter (2006), Great earthquakes of variable magnitude at the Cascadia subduction zone, *Quaternary Res.*, 65, 354-365.

Obara, K. (2002), Nonvolcanic deep tremor associated with subduction in southwest Japan, *Science*, 296, 1679-1681.

Obara, K., H. Hirose, F. Yamamizu, and K. Kasahara (2004), Episodic slow slip events accompanied by non-volcanic tremors in southwest Japan subduction zone, *Geophysical Research Letters*, 31(23), doi:10.1029/2004GL020848.

Okada, Y. (1992), Internal deformation due to shear and tensile faults in a half-space, *Bulletin of the Seismological Society of America*, *82*(2), 1018–1040.

Pacheco, J. F., L. R. Sykes, and C. H. Scholz (1993), Nature of seismic coupling along simple plate boundaries of the subduction type, *J. Geophys. Res.*, 98(8), 14, 133-14,159.

Persson, L. 2003, Statistical tests for regional seismic phase characterizations, *Journal of Seismology*, 7(1), 19-33.

Rogers, G. (2007, April). Episodic Tremor and Slip in Northern Cascadia–Going Back in Time, paper presented at the 2007 Seismol. Soc. Am. In *Annual Meeting, Waikoloa, Hawaii*, 11-13.

Rogers, G., and H. Dragert (2003), Episodic tremor and slip on the Cascadia subduction zone: The chatter of silent slip." *Science*, 300(5627), 1942-1943.

Rubinstein, J. L., J. Gomberg, J. E. Vidale, A. G. Wech, H. Kao, K. C. Creager, and G. Rogers (2009), Seismic wave triggering of nonvolcanic tremor, episodic tremor and slip, and earthquakes on Vancouver Island, *J. Geophys. Res.*, 114(B2), doi:10.1029/2008JB005875.

Satake, K., K. Wang, and B. F. Atwater (2003), Fault slip and seismic moment of the 1700 Cascadia earthquake inferred from Japanese tsunami descriptions, *J. Geophys. Res.*, 108(11), doi:10.1029/2003JB002521.

Scholz, C. H. (1990), The mechanics of earthquakes and faulting, Cambridge Univ. Press, Cambridge.

Segall, P., A. M. Rubin, A. M. Bradley, and J. R. Rice (2010), Dilatant strengthening as a mechanism for slow slip events, *J. Geophys. Res.,* 115(B12305), doi:10.1029/2010JB007449.

Shelly, D. R., G. C. Beroza, S. Ide, and S. Nakamula (2006), Low-frequency earthquakes in Shikoku, Japan, and their relationship to episodic tremor and slip, *Nature* 442, 188-191, doi:10.1038/nature04931.

Szeliga, W. M., T. M. Melbourne, M. M. Miller, and V. M. Santillan (2004), Southern Cascadia episodic slow earthquakes, *J. Geophys. Res.*, 31(L16602), doi:10.1029/2004GL020824.

Szeliga, W., T. Melbourne, V. Sanatillan, and M. Miller (2008), GPS constraints on 34 slow slip events within the Cascadia subduction zone, 1997–2005, *J. Geophys. Res.*, 113(B04404), doi:10.1029/2007JB004948.

Wech, A. G. (2010), Interactive tremor monitoring, *Seismological Research Letters*, 81(4), 664-669, doi:10.1785/gssrl.81.4.664.

Wech, A. G., and K. C. Creager (2007), Cascadia tremor polarization evidence for plate interface slip, *Geophysical Research Letters*, 34(22), doi:10.1029/2007GL031167.

Wech, A. G., and K. C. Creager (2008), Automated detection and location of Cascadia tremor, *Geophyical Research Letters*, 35(20), doi:10.1029/2008GL035458.

Wech, A. G., K. C. Creager, and T. I. Melbourne (2009), Seismic and geodetic constraints on Cascadia slow slip, *J. Geophys. Res.*, 114(B10), doi:10.1029/2008JB006090.

Witter, R. C., H. M. Kelsey, and E. Hemphill-Haley (2003), Great Cascadia earthquakes and tsunamis of the past 6700 years, Coquille River estuary, southern coastal Oregon, *GSA Bull.*, 115(10), 1289-1306, doi: 10.1130/B25189.1.

# APPENDIX

Table 1 lists the GPS surface displacement observations for the 2010 ETS event. Offsets were determined from fitting a hyperbolic tangent function to MEASURES and PANGA GPS time series using the methods outlined in Larson et al. [2004]. Table 2 lists the GPS surface displacement observations for the 2011 ETS event. Offsets were determined from fitting a hyperbolic tangent function to MEASURES and PANGA GPS time series using the methods outlined in Larson et al. [2004]. Table 3 lists the GPS surface displacement observations for the 2012 ETS event. Offsets were determined from fitting a hyperbolic tangent function to MEASURES and PANGA GPS time series using the methods outlined in Larson et al. [2004]. Table 4 lists the GPS surface displacement observations for the 2013 ETS event. Offsets were determined from fitting a hyperbolic tangent function to MEASURES and PANGA GPS time series using the methods outlined in Larson et al. [2004].

Table 1: List of GPS stations used to analyze the 2010 ETS event in northern Cascadia.

| Latitude | Longitude | Station Name | North Displacement (mm) | North Uncertainty (mm) | East Displacement (mm) | East Uncertainty (mm) | Vertical Displacement (mm) | Vertical Uncertainty (mm) |
|---|---|---|---|---|---|---|---|---|
| 48.389781 | 236.512530 | ALBH | -0.53 | 0.11 | -1.21 | 0.11 | -1.10 | 0.48 |
| 48.648533 | 236.548872 | PGC5 | -1.97 | 0.15 | -1.59 | 0.14 | 2.35 | 0.60 |
| 48.923164 | 236.295871 | SC04 | -1.58 | 0.17 | -1.58 | 0.14 | -2.62 | 0.62 |
| 48.544269 | 235.586942 | PTRF | -1.32 | 0.18 | -0.14 | 0.20 | -1.93 | 0.70 |
| 48.297855 | 235.375094 | NEAH | 0.27 | 0.23 | -1.12 | 0.14 | -1.45 | 0.71 |
| 48.062322 | 235.859126 | P403 | 0.26 | 0.23 | -0.92 | 0.16 | -1.46 | 0.57 |
| 48.059549 | 236.496722 | P435 | -0.25 | 0.26 | -0.03 | 0.16 | -1.01 | 0.64 |
| 48.045303 | 236.865653 | P436 | -0.65 | 0.14 | -0.65 | 0.13 | -0.51 | 0.56 |
| 48.010618 | 237.224134 | CHCM | -2.28 | 0.14 | -1.00 | 0.11 | -3.77 | 0.52 |
| 48.217311 | 237.314396 | COUP | -1.00 | 0.18 | -1.64 | 0.12 | 1.50 | 0.49 |
| 48.546195 | 236.992390 | SC02 | -0.87 | 0.12 | -0.47 | 0.11 | -0.71 | 0.42 |
| 48.708193 | 237.090697 | P439 | -0.61 | 0.13 | -0.67 | 0.12 | -0.96 | 0.38 |
| 48.856193 | 237.506659 | P440 | -1.46 | 0.16 | -0.22 | 0.15 | -2.18 | 0.60 |
| 48.521558 | 237.776153 | SEDR | -1.10 | 0.15 | -2.16 | 0.12 | -1.82 | 0.69 |
| 48.419148 | 237.329738 | P438 | -1.04 | 0.15 | -2.14 | 0.21 | -1.42 | 0.38 |
| 48.174067 | 237.858141 | ARLI | 0.09 | 0.13 | -0.10 | 0.11 | -0.20 | 0.45 |
| 48.001810 | 237.540843 | P437 | -0.39 | 0.12 | -1.82 | 0.11 | -2.54 | 0.51 |
| 47.898507 | 237.717818 | PFLD | 0.09 | 0.13 | -0.43 | 0.13 | 6.30 | 0.50 |
| 47.653977 | 237.690524 | SEAT | -0.10 | 0.13 | -2.50 | 0.18 | -0.03 | 0.45 |
| 47.802725 | 237.485415 | P426 | -0.35 | 0.12 | -0.94 | 0.16 | -1.04 | 0.51 |
| 47.105841 | 237.711535 | THUN | 0.26 | 0.10 | -1.69 | 0.09 | -1.35 | 0.34 |
| 47.172057 | 237.429195 | PCOL | -0.38 | 0.13 | -1.61 | 0.33 | -2.81 | 0.56 |
| 46.948717 | 237.394265 | YELM | -0.42 | 0.13 | -0.92 | 0.12 | -0.76 | 0.47 |
| 47.218786 | 237.241685 | LNGB | 0.36 | 0.13 | -0.51 | 0.11 | -0.07 | 0.42 |
| 47.391363 | 237.390540 | PRDY | -0.26 | 0.12 | -1.33 | 0.13 | -1.38 | 0.41 |

| | | | | | | | | |
|---|---|---|---|---|---|---|---|---|
| 47.497605 | 237.239416 | ELSR | -0.51 | 0.14 | 0.02 | 0.14 | 12.01 | 0.70 |
| 47.287904 | 237.058790 | P423 | 0.42 | 0.11 | 0.47 | 0.12 | -1.33 | 0.44 |
| 47.409299 | 236.633474 | P419 | -0.38 | 0.11 | -0.60 | 0.15 | 1.52 | 0.40 |
| 47.236645 | 236.592187 | P418 | -0.47 | 0.12 | -0.49 | 0.13 | -0.37 | 0.41 |
| 47.003844 | 236.563778 | P430 | 0.61 | 0.13 | -0.12 | 0.10 | 1.42 | 0.50 |
| 47.212800 | 235.795419 | PABH | -0.41 | 0.10 | -1.34 | 0.10 | 0.43 | 0.33 |
| 47.816587 | 236.294263 | SC03 | 0.80 | 0.23 | -2.60 | 0.13 | 4.09 | 0.38 |
| 47.766222 | 235.694104 | P402 | -0.30 | 0.11 | -0.40 | 0.11 | -0.31 | 0.38 |
| 47.937188 | 235.442982 | P401 | -0.25 | 0.11 | -0.54 | 0.09 | -1.43 | 0.38 |
| 48.835329 | 234.864896 | BAMF | -1.13 | 0.17 | -0.23 | 0.14 | -0.41 | 0.82 |
| 49.294811 | 235.913521 | NANO | -0.35 | 0.13 | -0.61 | 0.10 | -2.13 | 0.52 |
| 49.256329 | 235.139045 | PTAL | -0.58 | 0.21 | -0.10 | 0.14 | -2.80 | 0.67 |
| 48.925638 | 234.458360 | UCLU | -0.67 | 0.11 | -0.23 | 0.09 | 2.26 | 0.53 |
| 46.795486 | 236.977403 | GRMD | -0.29 | 0.17 | -0.13 | 0.13 | 2.01 | 0.51 |
| 46.531856 | 237.570772 | P421 | -0.90 | 0.15 | 0.20 | 0.12 | 9.95 | 0.62 |
| 46.452694 | 237.154602 | P425 | -0.10 | 0.11 | -0.49 | 0.10 | 0.81 | 0.41 |
| 46.207373 | 236.231637 | TPW2 | -1.65 | 0.22 | -2.08 | 0.14 | -0.26 | 0.50 |

Table 2: List of GPS stations used to analyze the 2011 ETS event in northern Cascadia.

| Latitude | Longitude | Station Name | North Displacement (mm) | North Uncertainty (mm) | East Displacement (mm) | East Uncertainty (mm) | Vertical Displacement (mm) | Vertical Uncertainty (mm) |
|---|---|---|---|---|---|---|---|---|
| 48.389781 | 236.512530 | ALBH | -0.71 | 0.14 | -1.22 | 0.16 | 2.09 | 0.52 |
| 48.648533 | 236.548872 | PGC5 | -0.79 | 0.18 | -0.86 | 0.15 | 0.43 | 0.50 |
| 48.923164 | 236.295871 | SC04 | -1.25 | 0.18 | -0.48 | 0.17 | -2.59 | 0.58 |
| 48.544269 | 235.586942 | PTRF | -0.86 | 0.16 | -0.30 | 0.16 | 1.91 | 0.59 |
| 48.297855 | 235.375094 | NEAH | -0.48 | 0.17 | -0.68 | 0.16 | -0.53 | 0.57 |
| 48.062322 | 235.859126 | P403 | 0.98 | 0.22 | -0.99 | 0.16 | 3.31 | 0.61 |
| 48.059549 | 236.496722 | P435 | -0.37 | 0.27 | -0.06 | 0.16 | 4.02 | 0.92 |
| 48.045303 | 236.865653 | P436 | -0.83 | 0.14 | 0.09 | 0.13 | 0.03 | 0.59 |
| 48.010618 | 237.224134 | CHCM | -0.28 | 0.13 | -0.68 | 0.13 | -2.59 | 0.56 |
| 48.217311 | 237.314396 | COUP | -0.17 | 0.16 | -0.34 | 0.15 | 0.37 | 0.52 |
| 48.546195 | 236.992390 | SC02 | -1.30 | 0.14 | -0.02 | 0.15 | 1.41 | 0.48 |
| 48.708193 | 237.090697 | P439 | 1.39 | 0.15 | -0.55 | 0.16 | 1.13 | 0.56 |
| 48.856193 | 237.506659 | P440 | -0.76 | 0.14 | -0.09 | 0.12 | 0.82 | 0.51 |
| 48.521558 | 237.776153 | SEDR | -1.40 | 0.18 | -1.59 | 0.12 | -0.64 | 0.72 |
| 48.419148 | 237.329738 | P438 | -0.74 | 0.14 | -0.05 | 0.12 | 0.61 | 0.51 |
| 48.174067 | 237.858141 | ARLI | 0.06 | 0.13 | 0.22 | 0.10 | -0.55 | 0.42 |
| 47.898507 | 237.717818 | PFLD | -0.56 | 0.14 | -1.20 | 0.14 | 7.47 | 0.65 |
| 47.944380 | 238.169184 | LKCP | -0.31 | 0.14 | -1.36 | 0.12 | 0.40 | 0.53 |
| 47.653977 | 237.690524 | SEAT | -0.68 | 0.12 | -2.14 | 0.13 | 0.62 | 0.39 |
| 47.802725 | 237.485415 | P426 | -0.70 | 0.16 | 0.04 | 0.12 | -0.30 | 0.49 |
| 47.105841 | 237.711535 | THUN | 0.34 | 0.12 | -1.62 | 0.12 | -0.34 | 0.34 |
| 47.172057 | 237.429195 | PCOL | -0.90 | 0.21 | -0.73 | 0.18 | -0.47 | 0.63 |
| 46.948717 | 237.394265 | YELM | -0.87 | 0.13 | -1.28 | 0.15 | -0.08 | 0.53 |
| 47.218786 | 237.241685 | LNGB | -0.32 | 0.15 | -1.43 | 0.12 | 0.49 | 0.46 |
| 47.391363 | 237.390540 | PRDY | -0.81 | 0.13 | -1.69 | 0.13 | -0.14 | 0.39 |

| | | | | | | | | |
|---|---|---|---|---|---|---|---|---|
| 47.497605 | 237.239416 | ELSR | -0.60 | 0.15 | -0.45 | 0.12 | 5.15 | 0.76 |
| 47.287904 | 237.058790 | P423 | -1.41 | 0.15 | -0.08 | 0.14 | -0.40 | 0.51 |
| 47.409299 | 236.633474 | P419 | -1.37 | 0.16 | -0.08 | 0.18 | 2.16 | 0.54 |
| 47.433920 | 236.387040 | P399 | -0.05 | 0.12 | 0.12 | 0.14 | 1.60 | 0.42 |
| 47.236645 | 236.592187 | P418 | -0.85 | 0.19 | -0.46 | 0.14 | 0.39 | 0.45 |
| 47.003844 | 236.563778 | P430 | -0.41 | 0.17 | -0.69 | 0.13 | 1.58 | 0.45 |
| 46.925785 | 236.083856 | P398 | -0.53 | 0.14 | 0.18 | 0.11 | 0.25 | 0.44 |
| 47.212800 | 235.795419 | PABH | -0.12 | 0.10 | -0.20 | 0.13 | 1.02 | 0.37 |
| 47.513349 | 236.187550 | P400 | -0.36 | 0.25 | -0.64 | 0.23 | 2.50 | 1.07 |
| 47.816587 | 236.294263 | SC03 | 1.04 | 0.26 | -2.01 | 0.14 | 4.67 | 0.39 |
| 47.766222 | 235.694104 | P402 | -0.93 | 0.14 | 0.15 | 0.12 | 0.52 | 0.51 |
| 47.937188 | 235.442982 | P401 | -1.09 | 0.12 | 0.31 | 0.12 | 1.65 | 0.46 |
| 46.840085 | 237.743482 | CPXF | 0.61 | 0.13 | -1.53 | 0.12 | 1.25 | 0.35 |
| 46.795486 | 236.977403 | GRMD | -1.00 | 0.19 | -0.03 | 0.15 | -0.63 | 0.62 |
| 46.655991 | 236.270315 | P415 | -0.42 | 0.16 | -2.77 | 0.15 | 4.70 | 0.51 |
| 46.574738 | 236.702071 | P417 | -1.48 | 0.16 | 0.07 | 0.14 | 1.91 | 0.51 |
| 46.588602 | 237.133669 | P420 | 0.47 | 0.15 | -1.17 | 0.11 | 2.16 | 0.41 |
| 46.531856 | 237.570772 | P421 | -1.01 | 0.15 | 1.12 | 0.15 | 9.17 | 0.62 |
| 46.452694 | 237.154602 | P425 | -0.45 | 0.13 | 0.11 | 0.12 | -0.62 | 0.49 |
| 46.421620 | 236.200840 | P397 | -0.42 | 0.21 | 0.25 | 0.18 | -0.87 | 0.45 |
| 46.207373 | 236.231637 | TPW2 | -1.79 | 0.21 | -1.89 | 0.17 | 1.55 | 0.56 |
| 46.200502 | 236.623414 | P408 | -0.08 | 0.13 | -2.03 | 0.19 | 3.67 | 0.52 |
| 45.309514 | 236.177105 | P396 | 0.16 | 0.17 | -0.06 | 0.17 | -2.70 | 0.55 |
| 45.221106 | 237.410899 | P412 | -0.66 | 0.11 | -0.49 | 0.10 | -1.35 | 0.45 |
| 45.170864 | 237.129948 | WDBN | -1.15 | 0.14 | -2.46 | 0.21 | -1.41 | 0.60 |
| 45.022280 | 236.142474 | P395 | 0.35 | 0.18 | -1.67 | 0.13 | -0.31 | 0.46 |
| 44.941203 | 236.897734 | P376 | -1.38 | 0.14 | -1.29 | 0.14 | -1.50 | 0.48 |
| 44.585247 | 235.938430 | P367 | -0.51 | 0.11 | -0.88 | 0.14 | -0.60 | 0.44 |

Table 3: List of GPS stations used to analyze the 2012 ETS event in northern Cascadia.

| Latitude | Longitude | Station Name | North Displacement (mm) | North Uncertainty (mm) | East Displacement (mm) | East Uncertainty (mm) | Vertical Displacement (mm) | Vertical Uncertainty (mm) |
|---|---|---|---|---|---|---|---|---|
| 48.389781 | 236.512530 | ALBH | -0.3 | 0.11 | -0.43 | 0.14 | -1.42 | 0.5 |
| 48.648533 | 236.548872 | PGC5 | -0.21 | 0.16 | -1.28 | 0.17 | 1.45 | 0.42 |
| 48.923164 | 236.295871 | SC04 | -0.33 | 0.21 | -2.04 | 0.23 | 0.26 | 0.63 |
| 48.297855 | 235.375094 | NEAH | 1.07 | 0.24 | -0.53 | 0.17 | -3.05 | 1.01 |
| 48.546195 | 236.992390 | SC02 | 0.35 | 0.2 | -0.81 | 0.21 | 0.53 | 0.45 |
| 48.708193 | 237.090697 | P439 | 0.41 | 0.15 | -0.19 | 0.18 | 0.71 | 0.57 |
| 48.856193 | 237.506659 | P440 | 0.18 | 0.14 | -1.24 | 0.15 | 1.47 | 0.45 |
| 48.521558 | 237.776153 | SEDR | -0.13 | 0.2 | -0.68 | 0.15 | -1.1 | 0.85 |
| 48.419148 | 237.329738 | P438 | 0.45 | 0.11 | 0.19 | 0.13 | 0.23 | 0.42 |
| 47.944380 | 238.169184 | LKCP | 0.47 | 0.16 | -0.9 | 0.11 | 0.68 | 0.53 |
| 47.653977 | 237.690524 | SEAT | -0.5 | 0.15 | -1.47 | 0.13 | 1.5 | 0.49 |
| 47.802725 | 237.485415 | P426 | 0.62 | 0.16 | -0.1 | 0.12 | -0.9 | 0.49 |
| 47.172057 | 237.429195 | PCOL | 0.93 | 0.15 | -2.93 | 0.18 | -1.74 | 0.61 |
| 47.287904 | 237.058790 | P423 | -0.42 | 0.16 | -0.43 | 0.14 | 0.51 | 0.58 |
| 47.236645 | 236.592187 | P418 | 0.35 | 0.12 | 0.04 | 0.13 | 2.2 | 0.39 |
| 47.003844 | 236.563778 | P430 | -1.19 | 0.16 | -0.95 | 0.13 | 0.22 | 0.47 |
| 46.925785 | 236.083856 | P398 | -0.5 | 0.11 | 0.23 | 0.1 | 1.28 | 0.43 |
| 47.212800 | 235.795419 | PABH | 0.33 | 0.11 | -0.11 | 0.09 | 1.3 | 0.48 |
| 47.513349 | 236.187550 | P400 | -0.17 | 0.23 | -0.29 | 0.25 | 2.34 | 1.25 |
| 47.816587 | 236.294263 | SC03 | 1.03 | 0.31 | -1.38 | 0.17 | 1.52 | 0.36 |
| 47.766222 | 235.694104 | P402 | 0.09 | 0.14 | -0.95 | 0.11 | 1.61 | 0.43 |
| 47.937188 | 235.442982 | P401 | -0.26 | 0.11 | -0.34 | 0.1 | 0.5 | 0.46 |
| 46.655991 | 236.270315 | P415 | -0.15 | 0.21 | -0.67 | 0.17 | 0.03 | 0.49 |
| 46.574738 | 236.702071 | P417 | -0.7 | 0.17 | -0.49 | 0.14 | 1.68 | 0.59 |
| 46.588602 | 237.133669 | P420 | 0.08 | 0.13 | -0.41 | 0.13 | 0.65 | 0.39 |

| | | | | | | | | |
|---|---|---|---|---|---|---|---|---|
| 46.531856 | 237.570772 | P421 | -1.47 | 0.17 | 0.95 | 0.12 | 10.6 | 0.63 |
| 46.452694 | 237.154602 | P425 | -0.5 | 0.14 | 1.16 | 0.11 | -0.24 | 0.49 |
| 46.421620 | 236.200840 | P397 | 0.13 | 0.18 | 0.49 | 0.15 | 0.64 | 0.45 |
| 46.207373 | 236.231637 | TPW2 | 1.09 | 0.2 | -0.82 | 0.13 | 0.09 | 0.48 |
| 46.200502 | 236.623414 | P408 | 0.08 | 0.15 | 0.2 | 0.14 | 0.17 | 0.49 |
| 45.834869 | 237.307163 | P414 | -0.03 | 0.11 | 1.08 | 0.11 | 0.39 | 0.68 |
| 45.537993 | 236.842584 | P411 | 0.63 | 0.15 | 0.6 | 0.13 | -0.47 | 0.58 |
| 48.835329 | 234.864896 | BAMF | -1.51 | 0.18 | -1.33 | 0.21 | 1.44 | 0.77 |
| 49.154143 | 234.092162 | TFNO | -0.53 | 0.18 | -0.24 | 0.23 | 3.12 | 0.82 |
| 49.256329 | 235.139045 | PTAL | 1.42 | 0.16 | -1.56 | 0.17 | 4.76 | 1.05 |
| 47.015905 | 237.077125 | TWHL | 0.43 | 0.2 | -1.43 | 0.17 | -2.33 | 0.57 |
| 49.294811 | 235.913521 | NANO | 0.21 | 0.15 | -1.59 | 0.11 | -2.98 | 0.47 |

Table 4: List of GPS stations used to analyze the 2013 ETS event in northern Cascadia.

| Latitude | Longitude | Station Name | North Displacement (mm) | North Uncertainty (mm) | East Displacement (mm) | East Uncertainty (mm) | Vertical Displacement (mm) | Vertical Uncertainty (mm) |
|---|---|---|---|---|---|---|---|---|
| 48.389781 | 236.512530 | ALBH | -3.38 | 0.16 | -1.62 | 0.19 | -0.53 | 0.64 |
| 48.174067 | 237.858141 | ARLI | -1.22 | 0.25 | -0.18 | 0.23 | -1.29 | 0.78 |
| 48.835329 | 234.864896 | BAMF | -3.65 | 0.31 | -1.35 | 0.28 | 5.32 | 1.13 |
| 48.820305 | 235.869116 | CLRS | -3.67 | 0.29 | -1.32 | 0.29 | -1.73 | 0.95 |
| 47.944380 | 238.169148 | LKCP | -0.65 | 0.24 | 0.66 | 0.26 | -2.22 | 0.89 |
| 49.154143 | 234.092162 | TFNO | -5.48 | 0.29 | -3.86 | 0.39 | 3.96 | 1.17 |
| 49.256329 | 235.139045 | PTAL | -2.72 | 0.25 | 0.53 | 0.25 | -1.64 | 0.75 |
| 48.648533 | 236.548872 | PGC5 | -3.95 | 0.26 | -1.31 | 1.57 | -3.15 | 0.74 |
| 48.923164 | 236.295871 | SC04 | -3.18 | 0.27 | -1.19 | 0.31 | -4.66 | 0.83 |
| 48.544269 | 235.586942 | PTRF | -4.45 | 0.29 | -1.63 | 0.25 | 0.54 | 0.83 |
| 48.062322 | 235.859126 | P403 | -2.14 | 0.28 | -1.95 | 0.29 | 0.51 | 0.88 |
| 48.059549 | 236.496722 | P435 | -2.10 | 0.29 | -1.15 | 0.34 | 2.55 | 0.98 |
| 48.045303 | 236.865653 | P436 | -2.41 | 0.26 | -2.29 | 0.24 | -2.51 | 0.76 |
| 48.546195 | 236.992390 | SC02 | -3.78 | 0.26 | -1.86 | 0.23 | -3.22 | 0.72 |
| 48.708193 | 237.090697 | P439 | -3.61 | 0.26 | -1.63 | 0.23 | -3.61 | 0.64 |
| 48.856193 | 237.506659 | P440 | -1.57 | 0.24 | -1.04 | 0.23 | -4.33 | 0.67 |
| 48.521558 | 237.776153 | SEDR | -1.41 | 0.25 | -0.60 | 0.28 | -6.89 | 1.02 |
| 48.419148 | 237.329738 | P438 | -3.66 | 0.27 | -2.00 | 0.21 | -3.60 | 0.82 |
| 47.653977 | 237.690524 | SEAT | -1.54 | 0.23 | -0.47 | 0.20 | -6.57 | 0.71 |
| 47.513349 | 236.187550 | P400 | -1.14 | 0.52 | -1.35 | 0.36 | 2.91 | 1.62 |
| 47.816587 | 236.294263 | SC03 | -3.63 | 0.28 | -4.51 | 0.39 | 3.67 | 0.80 |
| 47.766222 | 235.694104 | P402 | -0.48 | 0.24 | -1.25 | 0.24 | -2.54 | 0.66 |
| 47.497605 | 237.239416 | ELSR | -0.63 | 0.26 | 0.26 | 0.20 | -0.37 | 0.21 |
| 47.433920 | 236.387040 | P399 | -0.07 | 0.26 | -3.72 | 0.18 | -2.02 | 0.62 |
| 47.969847 | 236.512296 | P064 | -4.53 | 0.24 | -1.38 | 0.23 | 4.11 | 0.93 |
| 48.010618 | 237.224134 | CHCM | -0.51 | 0.29 | -2.22 | 0.25 | -7.76 | 0.74 |

| | | | | | | | | |
|---|---|---|---|---|---|---|---|---|
| 48.001810 | 237.540843 | P437 | -1.81 | 0.22 | -1.69 | 0.26 | -4.73 | 0.72 |
| 47.755010 | 237.332584 | UFDA | -1.55 | 0.32 | -1.07 | 0.29 | -7.27 | 1.23 |
| 47.823184 | 237.125288 | P424 | -0.88 | 0.29 | -1.44 | 0.27 | -3.79 | 0.76 |
| 47.682300 | 237.684836 | SSHO | -1.42 | 0.25 | -1.25 | 0.25 | -10.42 | 0.84 |
| 48.417854 | 237.662798 | VERN | -1.56 | 0.24 | -2.32 | 0.25 | -4.88 | 0.66 |
| 49.294811 | 235.913521 | NANO | -1.89 | 0.23 | -1.73 | 0.23 | 6.09 | 0.83 |
| 49.592363 | 233.383389 | NTKA | -0.245 | 0.244 | -2.110 | 0.261 | -1.640 | 0.825 |